Time-Dependent Integral Neutron Transport for Inertial Confinement Fusion

C.S. Aplin and D.L. Henderson

August 2007

UWFDM-1332

FUSION TECHNOLOGY INSTITUTE

UNIVERSITY OF WISCONSIN

MADISON WISCONSIN

Time-Dependent Integral Neutron Transport for Inertial Confinement Fusion

C.S. Aplin and D.L. Henderson

Fusion Technology Institute
University of Wisconsin
1500 Engineering Drive
Madison, WI 53706

http://fti.neep.wisc.edu

August 2007

UWFDM-1332

Table of Contents

List of Tables

List of Figures

Chapter 1. Introduction

1.1 Introduction to Fusion

Fusion energy, which has the potential to create vast amounts of energy, has been under development since the 1950's. The two major advantages of fusion energy over current forms of energy production are: 1) a major component of fusion fuel, deuterium, is plentiful and inexpensive, and 2) the waste produced from fusion is not made up of long-lived, heavy radioactive isotopes, but stable light isotopes such as hydrogen and helium [1]. A disadvantage, however, is that the flux of neutrons produced from the fusion reactions can activate reactor structural materials. In contrast to waste from fission reactors, however, there is no transuranic waste. Though a few radioisotopes created are long-lived, the vast majority of radioisotopes have short half-lives, and the small inventory of radioactive waste will decrease rapidly.

Fusion is the process of combining the nuclei of two light elements together, creating a heavier element. Fusion has been difficult to achieve because the nuclei are both positively charged, and therefore repel each other. The fusion fuel must be heated to incredibly high temperatures such that the velocities of the nuclei are very large, allowing the nuclei to overcome the repulsive Coulomb force. The nuclei will scatter off of each other more often then they will fuse together, therefore the fuel must be confined, allowing the nuclei to collide many millions of times, until they finally fuse [1].

There are two confinement schemes commonly considered for fusion energy. These are the magnetic and inertial confinement fusion concepts. The goal of magnetic confinement fusion is to create a steady-state plasma confined by a magnetic field [2]. Devices currently being considered for magnetic confinement are the Tokamak and the Stellator designs [1]. Inertial confinement fusion involves heating the fusion fuel to thermonuclear temperatures by rapid compression of the fuel pellet so that a large number of fusion reactions occur before the pellet blows apart. Large laser beam generators or light/heavy ion beam accelerators are used as drivers to generator beams, which compress the pellets to high densities and the fuel to thermonuclear temperatures

[1]. While the fusion reactions considered for the two concepts are the same, the density and pressure regimes differ by several orders of magnitude [2].

1.2 Introduction to Inertial Confinement Fusion

Unlike magnetic confinement fusion, Inertial Confinement Fusion, or ICF, does not depend on external means to confine a plasma. Instead, ICF utilizes the mass inertia of the fuel to confine the fuel long enough to achieve thermonuclear burn. The confinement time of an ICF plasma is then very short, usually on the order of 50 ps. Target compression influences the confinement time and the burn yield. Compression to extremely high densities leads to longer confinement times and high reaction rates [2].

To protect the walls of the reactor vessel in which the fusion burn takes place, the energy release from the explosion of the fuel must be limited. This in turn limits the mass of fuel in a pellet to only 1 - 10 mg. To burn such a small mass of fuel requires a very high fuel compression [2].

A typical deuterium-tritium fuel pellet consists of three regions, as seen in Figure 1.1. The outer shell of the pellet is an ablator, and is made of plastic. Behind this is a shell of deuterium-tritium ice, and the inner most region is deuterium-tritium vapor. The pellet is uniformly irradiated by a large number of lasers. The energy from the lasers heats up the ablator, which begins to expand. To conserve momentum, the rest of the shell is forced inward. As the fuel pressure increases from the implosion, a hot spot of very high temperature is formed at the center of the pellet. Energy loss due to conduction by electrons and radiation from the hot spot to the surrounding cold fuel cool the hot spot [2].

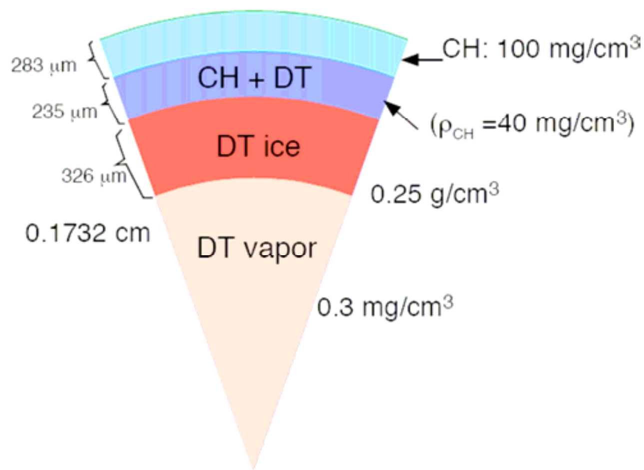

Figure 1. 1: ICF Fuel Pellet. Credit: Andy Schmitt, Naval Research Laboratory

As long as losses due to conduction and radiation are not too high, ignition will occur in the central hot spot. To achieve ignition, the confinement parameter, ρ*R, of the hot spot must be equal to about 0.3 g/cm^2, where ρ is the density and R is the radius [3]. Alpha particles, produced from fusion reactions in the hot spot, propagate the burn by depositing their energy in the surrounding fuel. Meanwhile, the fuel is rapidly expanding, and remains confined for only about 50 ps. Because the fusion products can be used to propagate the burn to the surrounding fuel, only the hot spot needs to be compressed to a very high density at a very high temperature, which in turn requires less input energy from the lasers [2].

1.3 Motivating Neutron Transport

Neutron transport is of great importance to the study of Inertial Confinement Fusion. High-energy neutrons are born from the fusion process. These particles, along with alpha particles, are necessary to propagate the burn from the ignition region to the outlying low-temperature, high-density regions surrounding the ignition region of the target.

The following reactions use the most common fusion fuels, deuterium, tritium, and helium-3, and therefore are of importance to ICF devices:

$D + T \rightarrow {}^4He$ (2.5 MeV) + n (14.1 MeV)

$D + D \rightarrow T$ (1.0 MeV) + H (2.0 MeV)

$D + D \rightarrow {}^3He$ (0.8 MeV) + n (2.45 MeV)

$D + {}^3He \rightarrow {}^4He$ (2.6 MeV) + H (14.7 MeV)

As can be seen from the above reactions, neutrons figure prominently in fusion reactions. Neutrons result from two of the four reactions, and carry the bulk of the kinetic energy when present.

The alpha particles and neutrons created during a fusion burn propagate the burn by transferring energy to the low-temperature, high-density regions surrounding the ignition region. However, alpha particles and neutrons travel at different velocities. In a sense, neutrons can be thought of as pre-heating the areas that are later ignited by the energy from the alpha particles, an effect that may or may not be detrimental to the burn process. A complete understanding of the interplay of these particles is essential to fully characterize a fusion burn.

Accurate neutron modeling is important to ICF for other reasons, as well. The neutrons eventually transport out of the target and collide with the reactor vessel walls. Since the neutrons may suffer collisions before escaping the target, the neutrons emerge with a spectrum of energies. This fact will affect the radioactivity of the reactor vessel walls, tritium breeding, shield designs, and dose rates to reactor personnel.

The deuterium-tritium reaction is of great interest to ICF because the fuel mixture has the lowest ignition temperature and the highest specific yield of any of the above reactions [2]. However, since tritium has a half-life of only 12.3 years, tritium must be breed. The reactor vessel has specific zones designed for tritium breeding. Two important tritium-breeding reactions are:

${}^6Li + n \rightarrow T + \alpha + 4.86$ MeV

${}^7Li + n \rightarrow T + \alpha + n - 2.87$ MeV

Both these reactions require neutrons for breeding. However, the ${}^6Li$ reaction requires slow neutrons, while the ${}^7Li$ reaction requires fast neutrons. Therefore, it is important to know the energy spectrum of the neutrons escaping the target, to determine if the breeding zone must be enriched with ^{6}Li to ensure that enough tritium is breed.

1.4 Time-Dependent Neutron Transport

The burn time of a fusion target is incredibly fast, taking approximately 50 ps. During this phase, a fusion target fuel region changes rapidly. Given the speed of a 14.1 MeV neutron as roughly 5.2 cm/ns and the approximate radius of the compressed fuel target as 0.012 cm, the fuel transversal time for a neutron is found to be approximately 4.6 ps. Therefore, during the burn phase, a propagating neutron would encounter a rapidly changing medium. For this reason, a steady state approach to neutron transport study would not be appropriate.

On the other hand, since the fusion target is so small, a neutron would only experience a few collisions before escaping the target. The number of collisions a neutron would experience can be calculated from an escape probability estimate as a function of the target density, ρ, multiplied by the target radius, R. Such a study indicates that, for a $\rho{*}R$ value of 2.0 g/cm^2, less than 30% of the neutrons experience a collision [3]. The number of collisions a neutron experiences in a fusion target is small. Therefore, a Neumann series approach is considered appropriate for calculating the total neutron flux. As discussed in Section 2.1, a Neumann series decomposes the total flux into the uncollided flux and the collided fluxes. The first collided flux is calculated using the uncollided flux as a source term, the second collided flux is calculated using the first collided flux as a source term, and so on. Since the neutrons only make a few collisions before escaping the target, only the first several collided fluxes need to be calculated to obtain an accurate answer for the total flux.

As is evident from the above discussion, time-dependent neutron transport is important to ICF for many reasons. The ensuing chapters will discuss the different methods used to solve the neutron transport equation and the work currently undertaken to address the specific problem of neutron transport in an ICF device. The final chapter will detail the steps necessary to produce a neutron transport code that can by coupled into the BUCKY radiation hydrodynamics code.

Chapter 2. Preliminary Work

This chapter will discuss the benchmark solutions that have been verified, the infinite slab and infinite sphere geometries. For each of the benchmarks, the form of the integral transport equation to be solved is derived and numerical results are given. This is the starting point for the development of a time-dependent integral equation formulation.

2.1 Infinite Slab Geometry

2.1.1 *Mathematical Development*

A Green's function is derived for the integral form of the "reduced collision equations" for an infinite slab geometry with an arbitrary isotropic source, and will be used to determine the time-dependent neutron flux.

To derive the Green's function, we begin with the time-dependent differential transport equation in planar coordinates for a one-dimensional infinite medium with an arbitrary source, $Q(x,t)$:

$$\left(\frac{1}{v}\frac{\partial}{\partial t}+\mu\frac{\partial}{\partial x}+\Sigma\right)\Psi(x,\mu,t)=\frac{Q(x,t)}{2} \tag{2.1}$$

The differential form of the transport equation can be converted to an integral equation for the scalar flux through either the method of characteristics or Laplace transforms [4]. The time-dependent integral equation is then of the form

$$\Phi(x,t)=\int_0^t\int_{-\infty}^{\infty}K(x,x';t,t')Q(x',t')dx'\,dt' \tag{2.2}$$

where $K(x,x';t,t')$ is the time-dependent kernel and $Q(x',t')$ is the time-dependent source. The source $Q(x',t')$ consists of both the external source, $S(x,t)$, and the isotropically scattered source, $\Sigma_s(x)\phi(x,t)$. Inserting the explicit expressions for the planar geometry scalar flux kernel [4] and the time-dependent arbitrary source into equation (2.2), and expanding the integral, one obtains

$$\Phi(x,t) = \Sigma_s \int_0^t \int_{-\infty}^{\infty} \frac{e^{-\Sigma v(t-t')}}{2(t-t')} H\left(t - t' - \frac{|x-x'|}{v}\right) \Phi(x',t') dx' dt' + \Phi_0(x',t') \qquad (2.3)$$

where $\Phi_0(x,t)$ is the uncollided flux. The uncollided flux is calculated as

$$\Phi_0(x,t) = \int_0^t \int_{-\infty}^{\infty} \frac{e^{-\Sigma v(t-t')}}{2(t-t')} H\left(t - t' - \frac{|x-x'|}{v}\right) S(x',t') dx' dt' \qquad (2.4)$$

The above equation is applied to the case of a unit planar source of pulsed neutrons located at the origin of an infinite medium, $S(x,t) = S_0\delta(x)\delta(t)$. Using this source in equation (2.4), the uncollided flux is found to be:

$$\Phi_0(x,t) = \frac{S_0}{2}\left(\frac{e^{-\Sigma v t}}{t}\right) H\left(t + \frac{x}{v}\right) H\left(t - \frac{x}{v}\right). \qquad (2.5)$$

The above solution for the uncollided flux describes an outgoing planar wave of particles moving to the left and right. The neutrons are confined between the wavefronts at $x = vt$ and $x = -vt$ [4].

The Neumann series method is used to decompose the time-dependent integral equation into a series of equations for the individual collided fluxes. The integral equation for the n^{th} collided flux is

$$\Phi_n(x,t) = \Sigma_s \int_0^t \int_{-\infty}^{\infty} \frac{e^{-\Sigma v(t-t')}}{2(t-t')} H\left(t - t' - \frac{|x-x'|}{v}\right) \Phi_{n-1}(x',t') dx' dt' \qquad (2.6)$$

for $n \geq 1$. The reduced collision equation ansatz for the n^{th} collided flux has the form [5]:

$$\Phi_n(x,t) = \frac{S_0}{2}\left(\frac{e^{-\Sigma vt}}{t}\right)\left(\frac{(\Sigma_s vt)^n}{n!}\right)\Psi_n(x,t) \tag{2.7}$$

where $\Psi_0(x,t) = H\left(t+\frac{x}{v}\right)H\left(t-\frac{x}{v}\right)$. Inserting the ansatz into equation (2.6) and simplifying, the following expression is found:

$$\Psi_n(x,t) = \frac{n}{2}\int_0^t\int_{-\infty}^{\infty}\frac{1}{(t-t')vt'}H\left(t-t'-\frac{|x-x'|}{v}\right)\left(\frac{(t')^{n-1}}{t^{n-1}}\right)\Psi_{n-1}(x',t')dx'dt'. \tag{2.8}$$

Using the substitution $\Psi_n(x,t) = F_n(x,t)H\left(t+\frac{x}{v}\right)H\left(t-\frac{x}{v}\right)$, equation (2.8) becomes

$$\begin{aligned} &F_n(x,t)H\left(t+\frac{x}{v}\right)H\left(t-\frac{x}{v}\right) = \\ &\quad \frac{n}{2}\int_0^t\int_{-\infty}^{\infty}\frac{1}{(t-t')vt'}\left(\frac{(t')^{n-1}}{t^{n-1}}\right)F_{n-1}(x',t')H\left(t-t'-\frac{|x-x'|}{v}\right)H\left(t'+\frac{x'}{v}\right)H\left(t'-\frac{x'}{v}\right)dx'dt' \end{aligned} \tag{2.9}$$

where $F_0(x,t) = 1$. F_n is then the shape factor for the n^{th} collided flux.

Next the integration variables x' and t' are transformed to the η', τ' domain. The transformed variables are defined as $\tau' = \frac{t'}{t}$ and $\eta' = \frac{x'}{vt'}$. The Jacobian $\left|\frac{\partial(x',t')}{\partial(\eta',\tau')}\right|$ evaluates to $vt^2\tau'$. Substituting the transformed variables into equation (2.9) and extracting the step functions, the following is obtained:

$$F_n(\eta) = \left(\frac{n}{2}\right)\left[\int_{-1}^{\eta}\int_0^{\frac{1-\eta}{1-\eta'}}\frac{(\tau')^{n-1}}{(1-\tau')}F_{n-1}(\eta')d\tau'd\eta' + \int_{\eta}^{1}\int_0^{\frac{1+\eta}{1+\eta'}}\frac{(\tau')^{n-1}}{(1-\tau')}F_{n-1}(\eta')d\tau'd\eta'\right] \tag{2.10}$$

The shape factors, F_n, depend only on the variable η. This can be seen from the fact that $F_0 = 1$, and that the limits of integration only contain the variable η. As a result, the τ' integration can always be performed analytically. The numerical integration over the η' variable can be performed using simple integration methods, such as quadrature rules.

Equation (2.10) can be written more compactly in terms of kernels as:

$$F_n(\eta) = \frac{n}{2}\left[\int_{-1}^{\eta} K_{n,A}(\eta,\eta')F_{n-1}(\eta')d\eta' + \int_{\eta}^{1} K_{n,B}(\eta,\eta')F_{n-1}(\eta')d\eta'\right] \tag{2.11}$$

where

$$K_{n,A}(\eta,\eta') = \int_{0}^{\frac{1-\eta}{1-\eta'}} \frac{(\tau')^{n-1}}{(1-\tau')} d\tau' \tag{2.12}$$

and

$$K_{n,B}(\eta,\eta') = \int_{0}^{\frac{1+\eta}{1+\eta'}} \frac{(\tau')^{n-1}}{(1-\tau')} d\tau' \tag{2.13}$$

The kernels for each n can be computed analytically. For instance, the kernels for n = 1 are

$$K_{1,A}(\eta,\eta') = \ln(1-\eta') - \ln(\eta-\eta') \tag{2.14}$$

and

$$K_{1,B}(\eta,\eta') = \ln(1+\eta') - \ln(\eta'-\eta). \tag{2.15}$$

Additionally, the kernels for $n = 2$ are

$$K_{2,A}(\eta,\eta') = \ln(1-\eta') - \ln(\eta-\eta') - \frac{1-\eta}{1-\eta'} \tag{2.16}$$

and

$$K_{2,B}(\eta,\eta') = \ln(1+\eta') - \ln(\eta'-\eta) - \frac{1+\eta}{1+\eta'}. \tag{2.17}$$

A pattern in the form of the kernels appears likely from the above equations. Indeed, further computation of the kernels leads to the following:

$$K_{n,A}(\eta,\eta') = \ln(1-\eta') - \ln(\eta-\eta') - \sum_{i=2}^{n}\frac{1}{i-1}\left(\frac{1-\eta}{1-\eta'}\right)^{i-1} \quad \text{for } n \geq 2 \tag{2.18}$$

and

$$K_{n,B}(\eta,\eta') = \ln(1+\eta') - \ln(\eta'-\eta) - \sum_{i=2}^{n}\frac{1}{i-1}\left(\frac{1+\eta}{1+\eta'}\right)^{i-1} \quad \text{for } n \geq 2 \tag{2.19}$$

It is possible to compute the first few shape factors analytically. The resulting first and second collided flux shape factors are [6]:

$$F_1(\eta) = -2\left[\left(\frac{1+\eta}{2}\right)\ln\left(\frac{1+\eta}{2}\right) + \left(\frac{1-\eta}{2}\right)\ln\left(\frac{1-\eta}{2}\right)\right] \tag{2.20}$$

and

$$F_2(\eta) = \frac{-\pi^2}{2}\left(1+\eta^2\right) - 6\left(\frac{1+\eta}{2}\right)\ln\left(\frac{1+\eta}{2}\right) - 6\left(\frac{1-\eta}{2}\right)\ln\left(\frac{1-\eta}{2}\right) + 3\left(\frac{1+\eta}{2}\right)^2\left[\ln\left(\frac{1+\eta}{2}\right)\right]^2 + 3\left(\frac{1-\eta}{2}\right)^2\left[\ln\left(\frac{1-\eta}{2}\right)\right]^2 + 6\left(\frac{1+\eta}{2}\right)^2 \mathrm{Li}_2\left(\frac{1+\eta}{2}\right) + 6\left(\frac{1-\eta}{2}\right)^2 \mathrm{Li}_2\left(\frac{1-\eta}{2}\right) \tag{2.21}$$

where $\mathrm{Li}_2(z)$ is the dilogarithm function, and is defined as [7]:

$$\mathrm{Li}_2(z) = -\int_0^z \frac{\ln(1-z)}{z} dz\,. \tag{2.22}$$

The dilogarithm belongs to the class of functions known as polylogarithms, and is a polylogarithm of order two [7].

Since the n^{th} shape factor is calculated from the $(n\text{-}1)^{\text{th}}$ shape factor, the ability to find analytic solutions to the first few shape factors is expected to lead to smaller errors in the total collided flux calculations.

For a pulsed source in space and time, all that remains after finding the shape factors is to calculate the total collided flux in x and t space. The individual collided fluxes are constructed from the shape factors:

$$\Phi_n(x,t) = \frac{S_0}{2}\left(\frac{e^{-\Sigma vt}}{t}\right)\left(\frac{(\Sigma_s\, vt)^n}{n!}\right)F_n(x,t) \tag{2.23}$$

where $F_n(x,t) = F_n(\eta)$. The total collided flux is the sum of the uncollided and collided fluxes.

$$\Phi_{tot}(x,t) = \Phi_0 + \Phi_1 + \Phi_2 + \Phi_3 + \ldots = \sum_{n=0}^{\infty} \Phi_n(x,t) \tag{2.24}$$

where Φ_0 is the uncollided flux. For an arbitrary source in an infinite medium, the Green's function for the n^{th} collided flux, $G_n(x,t)$, is given by equation (2.23). Then the time-dependent n^{th} collided flux is given by

$$\Phi_n(x,t) = \int_{t'}\int_{V'} G_n(x,x';t,t')S(x',t')dx'\,dt' \tag{2.25}$$

The kernels, equations (2.14), (2.15), (2.18), and (2.19) are singular at the point $\eta = \eta'$. Using the subtraction of singularity method [8], discussed in Appendix A, the integral equation for the shape factor, equation (2.11), can be rewritten as:

$$F_n(\eta) = \frac{n}{2}\left[\begin{array}{l} F_{n-1}(\eta)\int_{-1}^{\eta} K_{n,A}(\eta,\eta')d\eta' + \int_{-1}^{\eta} K_{n,A}(\eta,\eta')[F_{n-1}(\eta') - F_{n-1}(\eta)]d\eta' + \\ \quad F_{n-1}(\eta)\int_{\eta}^{1} K_{n,B}(\eta,\eta')d\eta' + \int_{\eta}^{1} K_{n,B}(\eta,\eta')[F_{n-1}(\eta') - F_{n-1}(\eta)]d\eta' \end{array}\right] \tag{2.26}$$

The first and third integrals can be performed analytically. The second and fourth integrals must be performed numerically. However, these integrals are equal to zero at the singularity.

Inserting the form of the kernels above into the first and third integrals of equation (2.26) and performing the integration, the following results are found for the first few values of n:

$$K_{1,A}(\eta) = K_{1,B}(\eta) = -2\left[\left(\frac{1+\eta}{2}\right)\ln\left(\frac{1+\eta}{2}\right) + \left(\frac{1-\eta}{2}\right)\ln\left(\frac{1-\eta}{2}\right)\right] \tag{2.27}$$

$$K_{2,A}(\eta) = -2\left[\left(\frac{1+\eta}{2}\right)\ln\left(\frac{1+\eta}{2}\right)\right] \tag{2.28}$$

$$K_{2,B}(\eta) = -2\left[\left(\frac{1-\eta}{2}\right)\ln\left(\frac{1-\eta}{2}\right)\right] \tag{2.29}$$

$$K_{3,A}(\eta) = -2\left[\left(\frac{1+\eta}{2}\right)\ln\left(\frac{1+\eta}{2}\right)\right] - \frac{1-\eta}{2} + \frac{(1-\eta)^2}{4} \tag{2.30}$$

$$K_{3,B}(\eta) = -2\left[\left(\frac{1-\eta}{2}\right)\ln\left(\frac{1-\eta}{2}\right)\right] - \frac{1+\eta}{2} + \frac{(1+\eta)^2}{4} \tag{2.31}$$

For $n \geq 3$, a pattern emerges for the integration result of the kernels:

$$K_{n,A} = -2\left[\left(\frac{1+\eta}{2}\right)\ln\left(\frac{1+\eta}{2}\right)\right] + \sum_{i=3}^{n} \frac{-(1-\eta)}{(i-2)(i-1)} + \frac{(1-\eta)^{i-1}}{(i-2)(i-1)2^{i-2}} \quad \text{for } n \geq 3 \tag{2.32}$$

and

$$K_{n,B} = -2\left[\left(\frac{1-\eta}{2}\right)\ln\left(\frac{1-\eta}{2}\right)\right] + \sum_{i=3}^{n} \frac{-(1+\eta)}{(i-2)(i-1)} + \frac{(1+\eta)^{i-1}}{(i-2)(i-1)2^{i-2}} \quad \text{for } n \geq 3 \tag{2.33}$$

2.1.2 *Shape Factors*

Equation (2.26) now needs to be solved. The first and third integrals can be performed analytically, as shown above, while the second and fourth integrals must be computed numerically. The function to be solved for in equation (2.26), $F_n(\eta)$, appears only on the left-hand side of the equation. Therefore, simple numerical integration methods, such as Gaussian quadrature rules and the Chebyshev Polynomial Expansion, can be utilized. The numerical integration methods are discussed in more detail in Appendix B. Each shape factor, F_n, corresponds to the n^{th} collided flux. Shown in Figure 2.1 are the uncollided and first five shape factors.

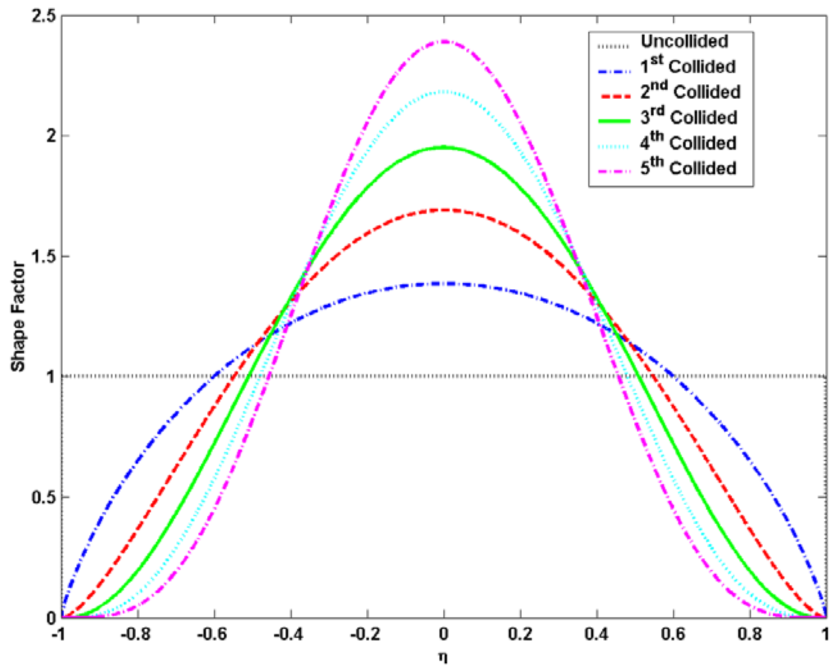

Figure 2. 1 Infinite Slab Shape Factors

From this figure, it is evident that, as n increases, the height of the shape factor at $\eta = 0$ increases, while the value of the shape factor near the boundaries goes to zero. It also appears that the area under the curves is conserved. To see if this is the case, the analytic functions for F_1 and F_2 were integrated over the range of η, [-1,1]. When these calculations were performed, it was found that the area under both curves was equal to two. It was expected that the area under the curves would be constant, since the shape factors only represent the scattering of neutrons. The absorption of neutrons is represented in the exponential decay term of the ansatz, equation (2.7), and is not included in the shape factors. Also, since the calculations were performed for an infinite medium, neutrons would not be lost through leakage.

The points $\eta = \pm 1$ are the wavefronts of the neutrons, and correspond to the points $x = \pm vt$. As expected, only the uncollided shape factor is non-zero at the wavefront. As the number of collisions increases, the domain on which the n^{th} shape factor is non-zero decreases. This trend continues, as shown by the n = 500 shape factor in Figure 2.2 below.

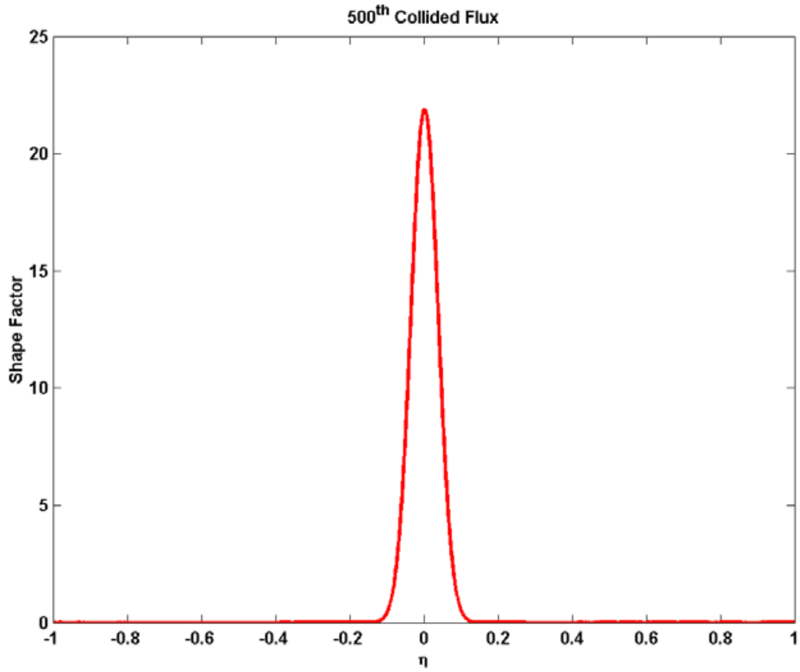

Figure 2. 2 500th Shape Factor

2.1.3 *Benchmark Results*

The n^{th} collided flux is calculated from the n^{th} shape factor using equation (2.23). The total flux for a pulsed source in time and space in an infinite medium is then calculated as a summation of the individual collided fluxes. For comparison to Ganapol's [9] and Olson's and Henderson's benchmark solutions [10], the following values were chosen: the source strength, $S_0 = 1$, the neutron velocity, $v = 1$, the total cross section, $\Sigma = 1$, and the absorption cross section, $\Sigma_a = 0$. For a given mean free time, t, the values for the distance, x_i, are calculated from:

$$x_i = vt\eta_i \tag{2.34}$$

Equation (2.34) shows that there is a one-to-one correlation between η and x; that is, if 2501 points are used for calculations in η space, then there will be 2501 points in x space. As time increases, the size of the x domain increases, while the size of the η

domain remains constant. Therefore, as time increases, the ratio of the length of the *x* domain to the number of *x* points decreases.

Shown in Figure 2.3 below is the total neutron flux at mean free time of 1, 3, 5, 7, and 9.

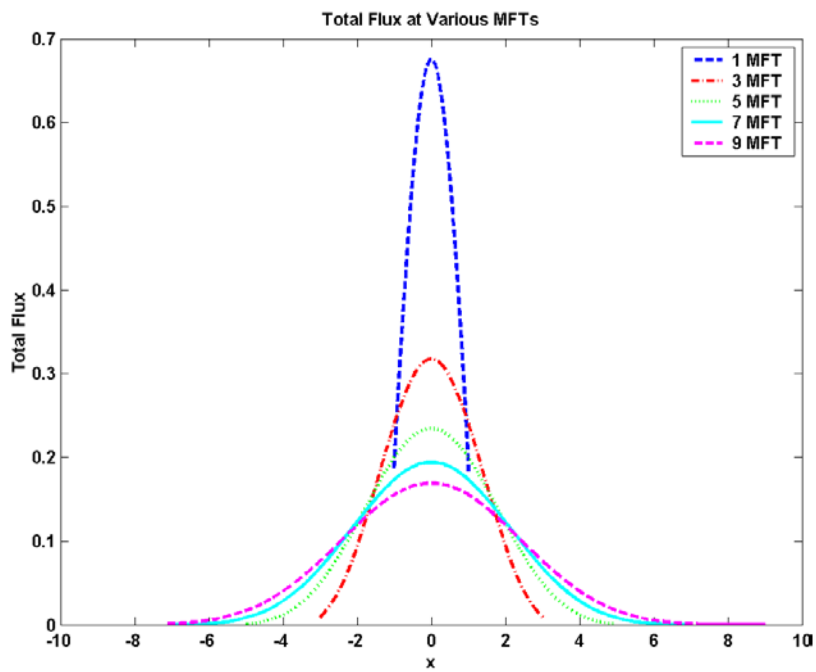

Figure 2. 3 Total Flux for Infinite Slab Benchmark at Various Mean Free Times

Shown in Table 2.1 below are the results for the infinite slab benchmark at small mean free times, compared to the results obtained by Ganapol, and by Olson and Henderson. Table 2.2 shows the benchmark solution at large mean free times.

Table 2. 1 Infinite Slab Geometry Benchmark Solution at Small Mean Free Times

Time	x	Flux, Ganapol	Flux, Olson and Henderson	Flux integral in η and τ
1	1	1.8394E-01	1.8394E-01	1.8394E-01
1	2	0.0000E+00	0.0000E+00	0.0000E+00
1	3	0.0000E+00	0.0000E+00	0.0000E+00
1	4	0.0000E+00	0.0000E+00	0.0000E+00
1	5	0.0000E+00	0.0000E+00	0.0000E+00
1	6	0.0000E+00	0.0000E+00	0.0000E+00
3	1	2.3942E-01	2.3942E-01	2.3942E-01
3	2	9.3836E-02	9.3835E-02	**9.3837E-02**
3	3	8.2978E-03	8.2978E-03	8.2978E-03
3	4	0.0000E+00	0.0000E+00	0.0000E+00
3	5	0.0000E+00	0.0000E+00	0.0000E+00
3	6	0.0000E+00	0.0000E+00	0.0000E+00
5	1	1.9957E-01	1.9957E-01	1.9957E-01
5	2	1.2105E-01	1.2105E-01	1.2105E-01
5	3	4.9595E-02	4.9595E-02	4.9595E-02
5	4	1.1823E-02	1.1823E-02	1.1823E-02
5	5	6.7379E-04	6.7379E-04	6.7379E-04
5	6	0.0000E+00	0.0000E+00	0.0000E+00
7	1	1.7347E-01	1.7347E-01	**1.7348E-01**
7	2	1.2293E-01	1.2293E-01	1.2293E-01
7	3	6.8028E-02	6.8028E-02	6.8028E-02
7	4	2.8447E-02	2.8447E-02	2.8447E-02
7	5	8.4158E-03	8.4157E-03	8.4158E-03
7	6	1.5036E-03	1.5036E-03	**1.5037E-03**
9	1	1.5528E-01	1.5528E-01	1.5528E-01
9	2	1.1935E-01	1.1935E-01	1.1935E-01
9	3	7.6384E-02	7.6384E-02	**7.6385E-02**
9	4	4.0186E-02	4.0186E-02	**4.0185E-02**
9	5	1.7004E-02	1.7004E-02	1.7004E-02
9	6	5.5765E-03	5.5764E-03	5.5765E-03

Table 2. 2 Infinite Slab Geometry Benchmark Solution at Large Mean Free Times

Time	x	Flux, Ganapol	Flux, Olson and Henderson	Flux integral in η and τ
15	1	1.2269E-01	1.2269E-01	1.2269E-01
15	2	1.0514E-01	1.0514E-01	1.0514E-01
15	3	8.1158E-02	8.1159E-02	8.1159E-02
15	4	5.6305E-02	5.6305E-02	5.6305E-02
15	5	3.4985E-02	3.4985E-02	3.4985E-02
15	6	1.9376E-02	1.9376E-02	1.9376E-02
25	1	9.6128E-02	9.6128E-02	9.6129E-02
25	2	8.7720E-02	8.7720E-02	**8.7721E-02**
25	3	7.5287E-02	7.5287E-02	7.5287E-02
25	4	6.0744E-02	6.0744E-02	6.0744E-02
25	5	4.6042E-02	4.6042E-02	4.6042E-02
25	6	3.2757E-02	3.2757E-02	3.2757E-02
35	1	8.1632E-02	8.1632E-02	8.1632E-02
35	2	7.6491E-02	7.6491E-02	7.6491E-02
35	3	6.8624E-02	6.8624E-02	6.8624E-02
35	4	5.8937E-02	5.8937E-02	5.8937E-02
35	5	4.8445E-02	4.8445E-02	**4.8444E-02**
35	6	3.8099E-02	3.8099E-02	3.8099E-02
45	1	7.2182E-02	7.2182E-02	7.2182E-02
45	2	6.8630E-02	6.8630E-02	6.8630E-02
45	3	6.3091E-02	6.3091E-02	6.3091E-02
45	4	5.6074E-02	5.6074E-02	**5.6073E-02**
45	5	4.8177E-02	4.8177E-02	**4.8176E-02**
45	6	4.0007E-02	4.0007E-02	4.0007E-02

2.2 Infinite Spherical Geometry

2.2.1 *Mathematical Development*

To derive the Green's function for the infinite spherical medium case, we begin with the time-dependent differential transport equation in spherical coordinates for a one-dimensional infinite medium with an arbitrary source, $Q(r,t)$:

$$\left(\frac{1}{v}\frac{\partial}{\partial t}+\mu\frac{\partial}{\partial r}+\frac{1-\mu^2}{r}\frac{\partial}{\partial \mu}+\Sigma\right)\Psi(r,\mu,t)=\frac{Q(r,t)}{2} \tag{2.35}$$

As in the slab case, the differential form of the transport equation can be converted to an integral equation for the scalar flux through either the method of characteristics or Laplace transforms [4]. The time-dependent integral equation is then of the form

$$\Phi(x,t) = \int_0^t \int_0^\infty K(r,r';t,t')Q(r',t')dr'\,dt' \tag{2.36}$$

where $K(r,r';t,t')$ is the time-dependent kernel and $Q(r',t')$ is the time-dependent source. The source $Q(r',t')$ consists of both the external source, $S(r',t')$, and the isotropically scattered source, $\Sigma_s(r')\phi(r',t')$. Inserting the explicit expressions for the spherical shell scalar flux kernel [4] and the time-dependent arbitrary source into equation (2.36), and expanding the integral, one obtains

$$\begin{aligned}\Phi(r,t) = \Sigma_s \int_0^t \int_0^\infty \frac{e^{-\Sigma v(t-t')}}{8\pi r r'(t-t')}\left[H\left(t-t'-\frac{|r-r'|}{v}\right) - H\left(t-t'-\frac{|r+r'|}{v}\right)\right]\times \\ \times \Phi(r',t')4\pi r'^2\,dr'\,dt' + \Phi_0(r,t)\end{aligned} \tag{2.37}$$

where $\Phi_0(r,t)$ is the uncollided flux. The uncollided flux is calculated using the point source kernel as:

$$\Phi_0(x,t) = \int_0^t \int_0^\infty \frac{e^{-\Sigma v(t-t')}}{4\pi|\vec{r}-\vec{r}'|(t-t')v}\,\delta\left(t-t'-\frac{|\vec{r}-\vec{r}'|}{v}\right)S(r',t')dr'\,dt' \tag{2.38}$$

The above equation is applied to the case of a unit point source of pulsed neutrons located at the origin of an infinite medium, $S(r,t) = \frac{S_0}{4\pi r^2}\delta(r)\delta(t)$. Using this source in equation (2.38), the uncollided flux is found to be:

$$\Phi_0(r,t) = \frac{S_0}{4\pi r v t}\left(\frac{e^{-\Sigma v t}}{t}\right)\delta\left(1-\frac{r}{vt}\right). \tag{2.39}$$

The above solution for the uncollided flux describes an outgoing pulse of neutrons that is infinite at the wavefront and zero elsewhere. The uncollided flux has a strong singularity at the wavefront, and the first collided flux will inherit this.

The Neumann series method is used to decompose the time-dependent integral equation, equation (2.37), into a series of equations for the individual collided fluxes. The integral equation for the n^{th} collided flux is

$$\begin{aligned}\Phi_n(r,t) = \Sigma_s \int_0^t\int_0^\infty \frac{e^{-\Sigma v(t-t')}}{8\pi r r'(t-t')}\left[H\left(t-t'-\frac{|r-r'|}{v}\right) - H\left(t-t'-\frac{|r+r'|}{v}\right)\right]\times \\ \times\Phi_{n-1}(r',t')4\pi r'^2\, dr'\, dt'\end{aligned} \tag{2.40}$$

for $n \geq 1$.

Equation (2.40) can be used to calculate each collided flux. However, there is quicker way to calculate the collided fluxes if the planar collided fluxes are known. The following relation allows for the transformation from slab geometry fluxes to spherical geometry fluxes, and is a simple way to obtain the spherical fluxes [11]:

$$\Phi_{n,sp}(r,t) = \frac{1}{2\pi r}\frac{\partial}{\partial r}\Phi_{n,pl}(r,t) \tag{2.41}$$

Using this relation and the planar forms for the first and second collided fluxes, the spherical fluxes are

$$\Phi_1(r,t) = \frac{S_0}{4\pi r}\frac{1}{vt}\left(\frac{e^{-\Sigma v t}}{t}\right)H\left(t-\frac{r}{v}\right)\ln\left(\frac{1+{r}/{vt}}{1-{r}/{vt}}\right) \tag{2.42}$$

and

$$\Phi_2(r,t)=\frac{S_0}{4\pi r}\frac{1}{vt}\left(\frac{e^{-\Sigma vt}}{t}\right)\frac{(\Sigma_s vt)^2}{2}H\left(t-\frac{r}{v}\right)\left[\pi^2\frac{r}{vt}+\frac{3}{2}\left(1-\frac{r}{vt}\right)\ln\left(\frac{1-{r}/{vt}}{2}\right)^2-\right.$$
$$\left.\frac{3}{2}\left(1+\frac{r}{vt}\right)\ln\left(\frac{1+{r}/{vt}}{2}\right)^2+3\left(1-\frac{r}{vt}\right)\mathrm{Li}_2\left(\frac{1-{r}/{vt}}{2}\right)-3\left(1+\frac{r}{vt}\right)\mathrm{Li}_2\left(\frac{1+{r}/{vt}}{2}\right)\right] \tag{2.43}$$

These solutions agree with the results found in literature [9, 10], but were found through alternate means.

Returning back to equation (2.40), the reduced collision equation ansatz for the n^{th} collided flux has the form:

$$\Phi_n(r,t)=\frac{S_0}{2}\left(\frac{e^{-\Sigma vt}}{t}\right)\left(\frac{(\Sigma_s vt)^n}{n!}\right)\frac{1}{(vt)^2}H\left(t-\frac{r}{v}\right)F_n(r,t) \tag{2.44}$$

where

$$F_1(r,t)=\frac{vt}{2\pi r}(\Sigma_s vt)\ln\left(\frac{1-{r}/{vt}}{1+{r}/{vt}}\right) \tag{2.45}$$

and

$$F_2(r,t)=\frac{vt}{2\pi r}\left[\pi^2\frac{r}{vt}+\frac{3}{2}\left(1-\frac{r}{vt}\right)\ln\left(\frac{1-{r}/{vt}}{2}\right)^2-\frac{3}{2}\left(1+\frac{r}{vt}\right)\ln\left(\frac{1+{r}/{vt}}{2}\right)^2+\right.$$
$$\left.3\left(1-\frac{r}{vt}\right)\mathrm{Li}_2\left(\frac{1-{r}/{vt}}{2}\right)-3\left(1+\frac{r}{vt}\right)\mathrm{Li}_2\left(\frac{1+{r}/{vt}}{2}\right)\right]. \tag{2.46}$$

Since the first collided flux, equation (2.42) has a singularity at $r = vt$, the numerical calculations must begin at $n = 3$, with the seconded collided flux as the forcing function.

Inserting the ansatz, equation (2.42) into the Neumann series expansion for the integral form of the time-dependent neutron transport equation and simplifying, the following expression is obtained for the n^{th} shape factor:

$$H\left(t-\frac{r}{v}\right)F_n(r,t)=\frac{n}{2}\int_0^t\int_0^\infty \frac{1}{vt'(t-t')}\left(\frac{t'}{t}\right)^{n-3}\frac{r'}{r}\left[H\left(t-t'-\frac{|r-r'|}{v}\right)-\right.$$
$$\left.H\left(t-t'-\frac{|r+r'|}{v}\right)\right]H\left(t'-\frac{r'}{v}\right)F_{n-1}(r',t')dr'dt' \tag{2.47}$$

Next the integration variables r' and t' are transformed to the η', τ' domain. The transformed variables are defined as $\tau'=\frac{t'}{t}$ and $\eta'=\frac{r'}{vt'}$. The Jacobian $\left|\frac{\partial(r',t')}{\partial(\eta',\tau')}\right|$ evaluates to $vt^2\tau'$. Substituting the transformed variables into equation (2.47) and extracting the step functions, the following equation for the n^{th} shape factor is obtained:

$$F_n(\eta)=\frac{n}{2}\left[\int_0^{\frac{1-\eta}{1-\eta'}}\int_0^{\eta}\frac{(\tau')^2}{1-\tau'}\frac{\eta'}{\eta}F_{n-1}(\eta')d\eta'd\tau'+\int_0^{\frac{1+\eta}{1+\eta'}}\int_\eta^1\frac{(\tau')^2}{1-\tau'}\frac{\eta'}{\eta}F_{n-1}(\eta')d\eta'd\tau'-\right.$$
$$\left.\int_0^{\frac{1-\eta}{1+\eta'}}\int_0^1\frac{(\tau')^2}{1-\tau'}\frac{\eta'}{\eta}F_{n-1}(\eta')d\eta'd\tau'\right]. \tag{2.48}$$

The notation may be simplified by introducing the concept of kernels:

$$F_n(\eta)=\frac{n}{2}\left[\int_0^\eta K_{A,n}(\eta,\eta')F_{n-1}(\eta')d\eta'+\int_\eta^1 K_{B,n}(\eta,\eta')F_{n-1}(\eta')d\eta'-\right.$$
$$\left.\int_0^1 K_{C,n}(\eta,\eta')F_{n-1}(\eta')d\eta'\right] \tag{2.49}$$

where the kernels are:

$$K_{A,n}(\eta,\eta')=\int_0^{\frac{1-\eta}{1-\eta'}}\frac{(\tau')^2}{1-\tau'}d\tau' \tag{2.50}$$

$$K_{B,n}(\eta,\eta') = \int_{0}^{\frac{1+\eta}{1+\eta'}} \frac{(\tau')^2}{1-\tau'} d\tau' \tag{2.51}$$

and

$$K_{C,n}(\eta,\eta') = \int_{0}^{\frac{1-\eta}{1+\eta'}} \frac{(\tau')^2}{1-\tau'} d\tau'. \tag{2.52}$$

The kernels can be calculated analytically. As in the planar coordinates case, the kernels follow a pattern with n and can be written as:

$$K_{A,n}(\eta,\eta') = \ln(1-\eta') - \ln(\eta-\eta') - \sum_{i=3}^{n} \frac{1}{n-2}\left(\frac{1-\eta}{1-\eta'}\right)^{n-2} \tag{2.53}$$

$$K_{B,n}(\eta,\eta') = \ln(1+\eta') - \ln(\eta'-\eta) - \sum_{i=3}^{n} \frac{1}{n-2}\left(\frac{1+\eta}{1+\eta'}\right)^{n-2} \tag{2.54}$$

and

$$K_{C,n}(\eta,\eta') = \ln(1+\eta') - \ln(\eta'+\eta) - \sum_{i=3}^{n} \frac{1}{n-2}\left(\frac{1+\eta}{1+\eta'}\right)^{n-2} \quad . \tag{2.55}$$

Examining the kernels, we see that $K_{A,n}$ and $K_{B,n}$ have a singularity at $\eta = \eta'$, while $K_{C,n}$ has a singularity at $\eta = \eta' = 0$. The singularities can be handled through the subtraction of singularity method. Using the subtraction of singularity method, the expression for F_n becomes:

$$F_n(\eta) = \frac{n}{2}\Bigg[\int_0^{\eta} K_{A,n}(\eta,\eta')\frac{\eta'}{\eta}\left[F_{n-1}(\eta') - F_{n-1}(\eta)\right]d\eta' + F_{n-1}(\eta)\int_0^{\eta} K_{A,n}(\eta,\eta')\frac{\eta'}{\eta}d\eta'$$
$$+\int_{\eta}^{1} K_{B,n}(\eta,\eta')\frac{\eta'}{\eta}\left[F_{n-1}(\eta') - F_{n-1}(\eta)\right]d\eta' + F_{n-1}(\eta)\int_{\eta}^{1} K_{B,n}(\eta,\eta')\frac{\eta'}{\eta}d\eta' \tag{2.56}$$
$$-\int_0^{1} K_{C,n}(\eta,\eta')\frac{\eta'}{\eta}\left[F_{n-1}(\eta') - F_{n-1}(\eta)\right]d\eta' - F_{n-1}(\eta)\int_0^{1} K_{C,n}(\eta,\eta')\frac{\eta'}{\eta}d\eta'\Bigg]$$

The second, fourth, and sixth integrals may always be performed analytically. Carrying out the integration, the following expressions are obtained for $n = 3$:

$$\int_0^{\eta} K_{A,3}(\eta,\eta')\eta' d\eta' = \frac{\eta}{2} - \frac{\eta^2}{2} + \frac{(1-\eta)^2}{2}\ln(1-\eta) - \frac{\eta^2}{2}\ln(\eta) \tag{2.57}$$

$$\int_{\eta}^{1} K_{B,3}(\eta,\eta')\eta' d\eta' = -\frac{1}{2} + \frac{\eta^2}{2} - \frac{(1+\eta)^2}{2}\ln(1+\eta) + \frac{(\eta^2-1)}{2}\ln(1-\eta) + (1+\eta)\ln 2 \tag{2.58}$$

$$\int_0^{1} K_{C,3}(\eta,\eta')\eta' d\eta' = -\frac{1}{2} + \frac{\eta}{2} - \frac{\eta^2}{2}\ln(\eta) + \frac{(\eta^2-1)}{2}\ln(1+\eta) + (1-\eta)\ln 2 \tag{2.59}$$

For $n = 4$, the integrals of the kernels may be written as:

$$\int_0^{\eta} K_{A,4}(\eta,\eta')\eta' d\eta' = -\frac{1}{2}\eta^2\ln(\eta) \tag{2.60}$$

$$\int_{\eta}^{1} K_{B,4}(\eta,\eta')\eta' d\eta' = \frac{\eta^2}{4} - \frac{1}{4} + \frac{(\eta^2-1)}{2}\ln(1-\eta) + \frac{(1-\eta^2)}{2}\ln 2 \tag{2.61}$$

$$\int_0^{1} K_{C,4}(\eta,\eta')\eta' d\eta' = \frac{\eta^2}{4} - \frac{1}{4} - \frac{\eta^2}{2}\ln(\eta) + \frac{(\eta^2-1)}{2}\ln(2) + \frac{(1-\eta^2)}{2}\ln 2 \tag{2.62}$$

Finally, for $n \geq 5$, a pattern in the integrals of the kernels emerges:

$$\int_0^{\eta} K_{A,n}(\eta,\eta')\eta' d\eta' = \left(1-\eta^2\right)\ln(1-\eta) - \frac{\eta^2}{2}\ln(\eta) + \sum_{i=5}^{n}\left[-\frac{(1-\eta)}{(i-2)(i-3)} + \frac{(1-\eta)^2}{(i-2)(i-4)} - \frac{(1-\eta)^{i-2}}{(i-2)(i-3)(i-4)}\right] \tag{2.63}$$

$$\int_{\eta}^{1} K_{B,n}(\eta,\eta')\eta' d\eta' = \frac{\eta^2}{4} - \frac{1}{4} + \frac{\left(\eta^2-1\right)}{2}\ln(1-\eta) + \frac{\left(1-\eta^2\right)}{2}\ln 2 + \sum_{i=5}^{n}\left[\frac{(1+\eta)}{(i-2)(i-3)} - \frac{(1+\eta)^2}{(i-2)(i-4)} + \frac{(1+\eta)^{i-2}}{(i-3)(i-4)2^{i-3}}\right. \tag{2.64}$$

$$\int_0^{1} K_{C,n}(\eta,\eta')\eta' d\eta' = \frac{\eta^2}{4} - \frac{1}{4} + \frac{\left(\eta^2-1\right)}{2}\ln(1+\eta) + \frac{\left(1-\eta^2\right)}{2}\ln 2 + \sum_{i=5}^{n}\left[\frac{(1-\eta)^{i-2}}{(i-2)}\left(\frac{2^{4-i}-1}{(i-4)} - \frac{2^{3-i}}{(i-3)}\right)\right] \tag{2.65}$$

The above expressions contain a singularity at the point $\eta = 0$. Appendix C shows the derivation of the expressions that must be solved for the n^{th} shape factor at $\eta = 0$. These expressions are reproduced below:

$$F_3(0) = \frac{3}{2}\left[2F_2(0)\ln 2 + \int_0^1 \left[F_2(\eta') - F_2(0)\right]\eta' \frac{2}{(1+\eta')\eta'} d\eta'\right] \tag{2.66}$$

$$F_4(0) = 2\left[F_3(0) + 2\int_0^1 \left[F_3(\eta') - F_3(0)\right]\eta' \left(\frac{1}{\eta'} - \frac{1}{1+\eta'} - \frac{1}{(1+\eta')^2}\right) d\eta'\right] \tag{2.67}$$

$$F_n(0) = \frac{n}{2}\left[F_{n-1}(0)\sum_{i=5}^{n}\left[\frac{(i-2)\left(16+2^i(i-5)\right)}{(i-3)(i-4)2^i}\right] + 2\int_0^1 \left[F_{n-1}(\eta') - F_{n-1}(0)\right]\eta' \left(\frac{1}{\eta'} - \sum_{i=3}^{v}\frac{1}{(i-2)(1+\eta')^{i-2}}\right) d\eta'\right] \tag{2.68}$$

3.2.2 *Shape Factors*

Equation (2.56) now needs to be solved. The second, fourth, and sixth integrals can be calculated analytically, while the first, third, and fifth integrals must be calculated numerically. Again, a simple numerical integration method can be implemented. The Clenshaw-Curtis quadrature rule was used for the first integral, while the Chebyshev Polynomial Expansion was used for the third and fifth integrals. At the point $\eta = 0$, equations (2.66), (2.67), and (2.68) must be solved, using either the Clenshaw-Curtis quadrature or the Chebyshev Polynomial Expansion. Shown in Figure 2.4 below are the first five collided shape factors. The uncollided flux, equation (2.39), is a delta function at the wavefront.

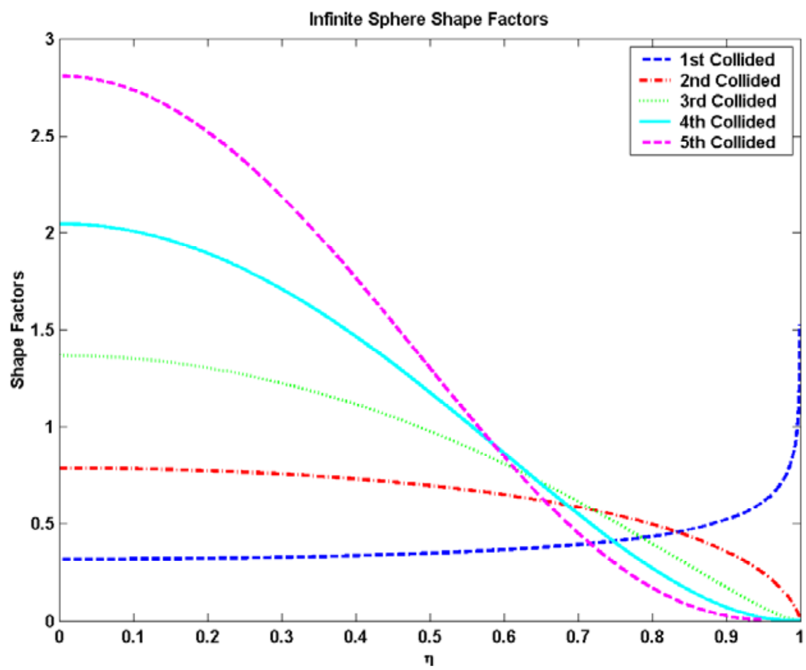

Figure 2. 4 Infinite Sphere Shape Factors

From this figure, it is apparent that the first collided flux has inherited the singularity from the uncollided flux at the wavefront. As in the infinite slab case, the collided fluxes, except for the first collided flux, go to zero at the wavefront. It should also be noted that the area under the curves of the collided fluxes increase, instead of staying constant, as in the slab case. This is because the area through which the neutrons travel increases as the area of a sphere, $4\pi r^2$.

Shown in Figure 2.5 below are the first five shape factors multiplied by the factor $4\pi\eta^2$. The area under these curves is equal to the volume integral of the shape factors. Therefore, the area under these curves is conserved, and equals two.

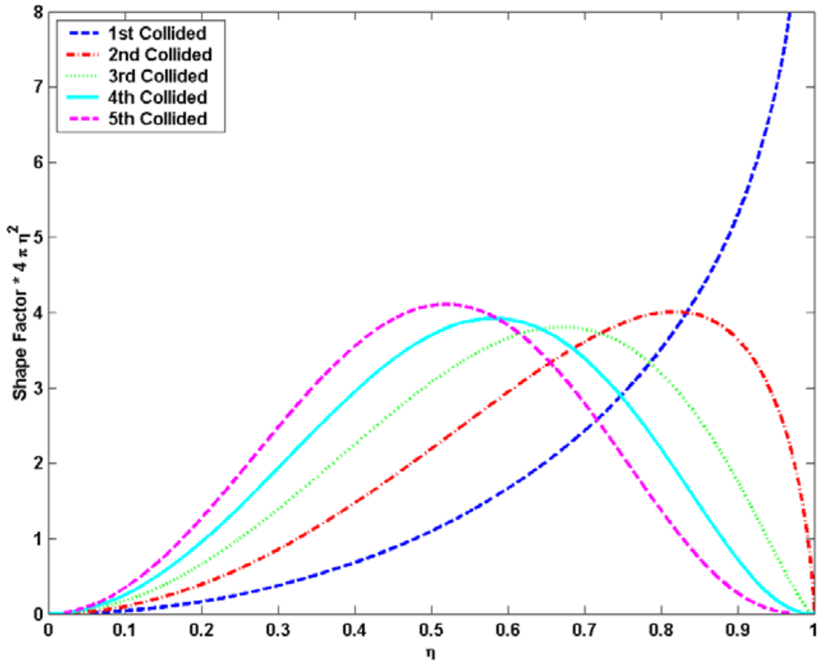

Figure 2. 5 Infinite Sphere Shape Factors Multiplied by η^2

2.2.3 *Benchmark Results*

The n^{th} collided flux is calculated from the n^{th} shape factor using equation (2.44). The total flux is again calculated as the sum of the individual collided fluxes. For comparison to Ganapol's [9] and Olson's and Henderson's benchmark solutions [10], the following values were chosen: the source strength, $S_0 = 1$, the neutron velocity, $v = 1$, the total cross section, $\Sigma = 1$, and the absorption cross section, $\Sigma_a = 0$. For a given mean free time, t, the values for the distance, r_i, are calculated from:

$$r_i = vt\eta_i \tag{2.69}$$

Again, there is a one-to-one correlation between η and r.

Shown in Figures 2.6 and 2.7 below is the total flux at early mean free times. From these figures, it is obvious how quickly the total flux falls off. These figures also show that the peak flux after 1 mean free time is at the origin.

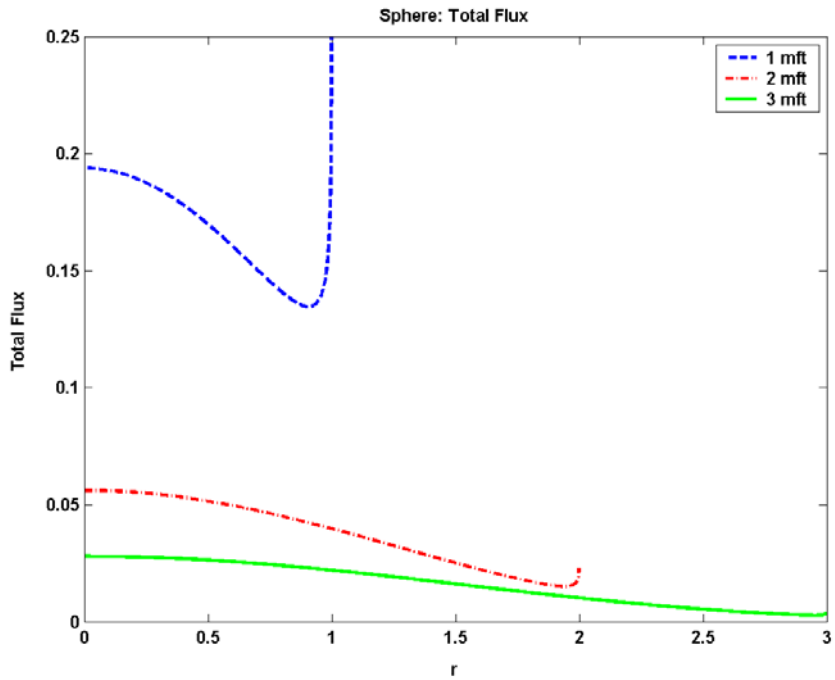

Figure 2. 6 Spherical Case Total Flux at Early Mean Free Times

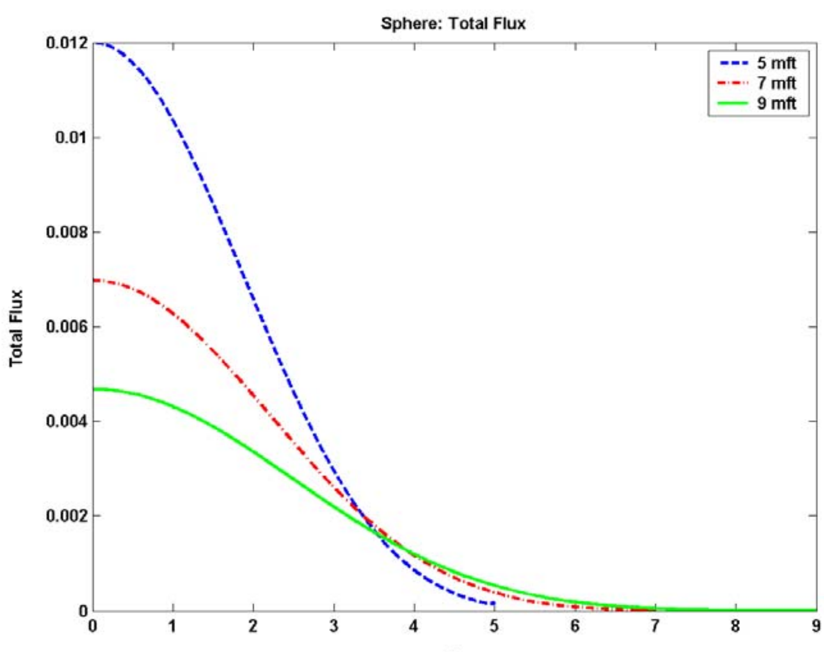

Figure 2. 7 Spherical Case Total Flux at Medium Mean Free Times

It is also instructive to graph the total flux multiplied by the geometry area, $4\pi r^2$. This is shown in figures 2.8 and 2.9 below. These figures show that the radius at which most of the neutrons are located increases with time.

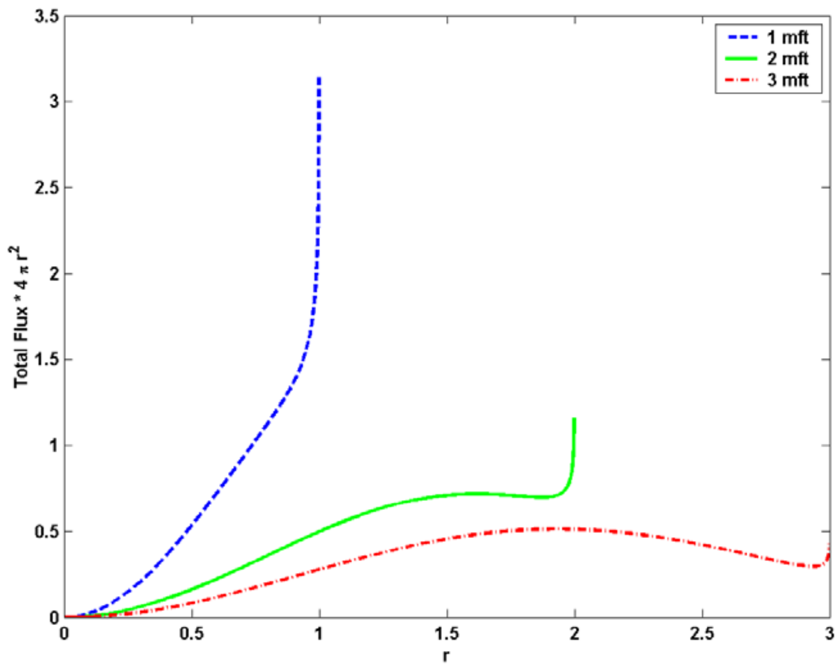

Figure 2. 8 Total Flux Multiplied by Area for Small Mean Free Times

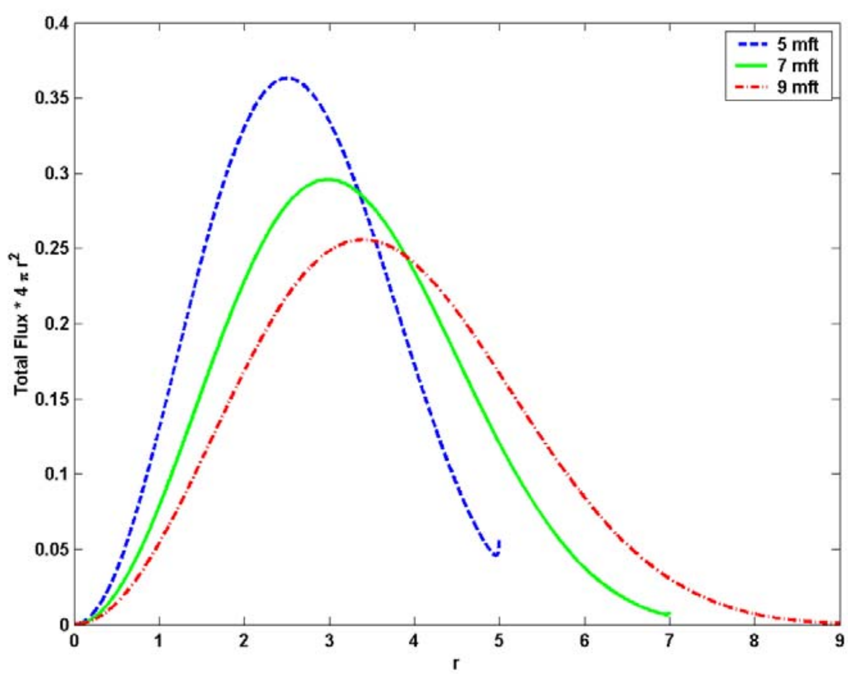

Figure 2. 9 Total Flux Multiplied by Area for Medium Mean Free Times

In figures 2.8 and 2.9, the singularity at the wavefront is much more pronounced.

The benchmark results, shown in comparison to Ganapol's and Olson's and Henderson's solutions, are shown in Table 2.3 for small mean free times, and Table 2.4 for large mean free times.

Table 2. 3 Infinite Sphere Geometry Benchmark Results at Small Mean Free Times

Time	r	Flux, Ganapol	Flux, Olson and Henderson	Flux integral in η and τ
1	1	Inf	Inf	Inf
1	2	0.0000E+00	0.0000E+00	0.0000E+00
1	3	0.0000E+00	0.0000E+00	0.0000E+00
1	4	0.0000E+00	0.0000E+00	0.0000E+00
1	5	0.0000E+00	0.0000E+00	0.0000E+00
1	6	0.0000E+00	0.0000E+00	0.0000E+00
3	1	2.2001E-02	2.2001E-02	2.2001E-02
3	2	1.0187E-02	1.0187E-02	1.0187E-02
3	3	Inf	Inf	Inf
3	4	0.0000E+00	0.0000E+00	0.0000E+00
3	5	0.0000E+00	0.0000E+00	0.0000E+00
3	6	0.0000E+00	0.0000E+00	0.0000E+00
5	1	1.0305E-02	1.0305E-02	1.0305E-02
5	2	6.5738E-03	6.5738E-03	**6.5739E-03**
5	3	2.9565E-03	2.9565E-03	2.9565E-03
5	4	8.5550E-04	8.5549E-04	8.5550E-04
5	5	Inf	Inf	Inf
5	6	0.0000E+00	0.0000E+00	0.0000E+00
7	1	6.2715E-03	6.2715E-03	6.2715E-03
7	2	4.5417E-03	4.5417E-03	4.5417E-03
7	3	2.6143E-03	2.6143E-03	**2.6144E-03**
7	4	1.1654E-03	1.1654E-03	1.1654E-03
7	5	3.8287E-04	3.8287E-04	3.8287E-04
7	6	8.3430E-05	8.3429E-05	8.3430E-05
9	1	4.3089E-03	4.3089E-03	4.3089E-03
9	2	3.3538E-03	3.3538E-03	3.3538E-03
9	3	2.1944E-03	2.1944E-03	2.1944E-03
9	4	1.1937E-03	1.1937E-03	1.1937E-03
9	5	5.3016E-04	5.3016E-04	5.3016E-04
9	6	1.8655E-04	1.8655E-04	1.8655E-04

Table 2. 4 Infinite Sphere Geometry Benchmark Results at Large Mean Free Times

Time	x	Flux, Ganapol	Flux, Olson and Henderson	Flux integral in η and τ
15	1	2.0059E-03	2.0059E-03	2.0059E-03
15	2	1.7263E-03	1.7263E-03	1.7263E-03
15	3	1.3423E-03	1.3423E-03	1.3423E-03
15	4	9.4107E-04	9.4106E-04	9.4107E-04
15	5	5.9294E-04	5.9294E-04	**5.9295E-04**
15	6	3.3430E-04	3.3430E-04	3.3430E-04
25	1	9.3283E-04	9.3283E-04	**9.3284E-04**
25	2	8.5252E-04	8.5252E-04	**8.5253E-04**
25	3	7.3353E-04	7.3353E-04	7.3353E-04
25	4	5.9394E-04	5.9394E-04	**5.9395E-04**
25	5	4.5228E-04	4.5228E-04	**4.5229E-04**
25	6	3.2364E-04	3.2363E-04	3.2364E-04
35	1	5.6323E-04	5.6323E-04	**5.6324E-04**
35	2	5.2816E-04	5.2815E-04	5.2816E-04
35	3	4.7444E-04	4.7443E-04	4.7444E-04
35	4	4.0819E-04	4.0819E-04	**4.0820E-04**
35	5	3.3630E-04	3.3629E-04	3.3630E-04
35	6	2.6523E-04	2.6523E-04	2.6523E-04
45	1	3.8637E-04	3.8637E-04	3.8637E-04
45	2	3.6752E-04	3.6752E-04	**3.6753E-04**
45	3	3.3812E-04	3.3812E-04	3.3812E-04
45	4	3.0083E-04	3.0083E-04	**3.0084E-04**
45	5	2.5882E-04	2.5882E-04	2.5882E-04
45	6	2.1530E-04	2.1529E-04	2.1530E-04

2.3 Error Analysis

This section discusses the error incurred in the numerical integration routines. The analysis is performed by assuming the benchmark solutions are as accurate as an analytic solution. The error is calculated using the Euclidian norm:

$$\varepsilon = \sqrt{\frac{\sum_{i=1}^{n} \left(\phi_{ana,i} - \phi_{cal,i}\right)^2}{N}} \tag{2.70}$$

where $\phi_{ana,i}$ is the benchmark value of the neutron scalar flux, $\phi_{cal,i}$ is the neutron scalar flux calculated above, i is the point in space and time at which the flux is given in the literature, and N is the total number of points at which the scalar fluxes are compared. The error is calculated relative to both Olson's and Ganapol's results. It is necessary to divide by the total number of points, N, since there are fewer points published in the literature for Ganapol's solution as for Olson's. By dividing by the number of points, the error calculations should be directly comparable.

2.3.1 *Error in Gauss-Legendre Quadrature Rule*

The number of quadrature points used in the Gauss-Legendre rule can be varied greatly. The quadrature rule is exact for polynomials of degree $2n$-1, where n is the number of quadrature points [12]. By varying both the number of quadrature points and the number of mesh points in η, an optimal combination of the two could be found using equation (2.70) as a measure for comparison. This procedure was carried out for both the infinite slab benchmark solution and the infinite spherical coordinates benchmark solution.

Shown in Table 2.5 below is the error for the Gauss-Legendre numerical integration scheme for various numbers of quadrature points and mesh points for the infinite slab case. Both the error relative to the Olson benchmark results and the error relative to the Ganapol benchmark results are shown. The lowest error, relative to both benchmark solutions, is for the configuration of 75 quadrature points and 2501 mesh points. The error relative to the Ganapol solution for this configuration was $1.5338*10^{-6}$, while the error relative to the Olson solution was $1.4747*10^{-6}$.

Shown in Table 2.6 below is the error for the Gauss-Legendre numerical integration scheme for the infinite spherical coordinates case. The lowest error relative to the Olson benchmark is $6.1846*10^{-8}$, for 60 quadrature points and 5001 mesh points. The lowest error relative to the Ganapol benchmark is $1.9626*10^{-8}$, for 60 quadrature points and 2501 mesh points. There is a fairly large difference between the error calculated relative to the Ganapol solution and the error calculated relative to the Olson solution. The cause of this is a point published only in the Olson solution that is believed to be in error. The point is at a mean free time of six and a mean free length of four. The value published in the Olson paper is $1.0665*10^{-3}$, while every simulation run with the above method returned $1.0655*10^{-3}$.

Table 2. 5 Gauss-Legendre Quadrature Error for Infinite Slab Case

Configuration	Error Relative Ganapol	Error Relative Olson	Configuration	Error Relative Ganapol	Error Relative Olson
30 Quadrature Points 2501 Mesh Points	1.5210E-05	1.6868E-05	40 Quadrature Points 5001 Mesh Points	3.4673E-06	4.3342E-06
40 Quadrature Points 2501 Mesh Points	4.1333E-06	5.9412E-06	50 Quadrature Points 5001 Mesh Points	1.9201E-06	2.0016E-06
50 Quadrature Points 2501 Mesh Points	8.2644E-06	9.2324E-06	60 Quadrature Points 5001 Mesh Points	3.2830E-06	3.4265E-06
60 Quadrature Points 2501 Mesh Points	1.6836E-06	1.5538E-06	75 Quadrature Points 5001 Mesh Points	1.8157E-06	2.0009E-06
75 Quadrature Points 2501 Mesh Points	**1.5338E-06**	**1.4747E-06**	30 Quadrature Points 7501 Mesh Points	1.0779E-05	1.2497E-05
80 Quadrature Points 2501 Mesh Points	2.3094E-06	2.5576E-06	40 Quadrature Points 7501 Mesh Points	3.8156E-06	4.5761E-06
90 Quadrature Points 2501 Mesh Points	2.2528E-06	2.3709E-06	50 Quadrature Points 7501 Mesh Points	2.1605E-06	2.2986E-06
100 Quadrature Points 2501 Mesh Points	3.1389E-06	3.6307E-06	60 Quadrature Points 7501 Mesh Points	1.7797E-06	1.7154E-06
30 Quadrature Points 5001 Mesh Points	1.1179E-05	1.2796E-05	75 Quadrature Points 7501 Mesh Points	2.2279E-06	2.1902E-06

Table 2. 6 Gauss-Legendre Quadrature Error for Infinite Spherical Coordinates Case

Configuration	Error Relative Ganapol	Error Relative Olson	Configuration	Error Relative Ganapol	Error Relative Olson
50 Quadrature Points 2501 Mesh Points	3.0123E-08	6.5709E-08	70 Quadrature Points 5001 Mesh Points	2.4495E-08	6.2026E-08
60 Quadrature Points 2501 Mesh Points	**1.9626E-08**	6.2319E-08	80 Quadrature Points 5001 Mesh Points	2.3998E-08	6.1914E-08
70 Quadrature Points 2501 Mesh Points	2.3014E-08	6.3742E-08	90 Quadrature Points 5001 Mesh Points	2.3805E-08	6.2599E-08
80 Quadrature Points 2501 Mesh Points	2.3014E-08	6.3742E-08	100 Quadrature Points 5001 Mesh Points	2.4037E-08	6.2683E-08
90 Quadrature Points 2501 Mesh Points	2.0184E-08	6.2732E-08	60 Quadrature Points 7501 Mesh Points	2.4721E-08	6.2058E-08
100 Quadrature Points 2501 Mesh Points	2.0230E-08	6.2668E-08	70 Quadrature Points 7501 Mesh Points	2.4037E-08	6.1935E-08
50 Quadrature Points 5001 Mesh Points	2.3844E-08	6.3029E-08	80 Quadrature Points 7501 Mesh Points	2.3960E-08	6.1867E-08
60 Quadrature Points 5001 Mesh Points	2.1082E-08	**6.1846E-08**	90 Quadrature Points 7501 Mesh Points	2.3921E-08	6.1881E-08

2.3.2 *Error in Chebyshev Polynomial Expansion*

The Chebyshev Polynomial Expansion method and Clenshaw-Curtis quadrature rule for numerical integration, discussed in Appendix B.2, are exact for polynomials of degree n. This is in contrast to the Gauss-Legendre rule, which is exact for polynomials of degree $2n$-1 [12]. This is not necessarily detrimental to the accuracy of the numerical integration, however, since the integrands being evaluated are not polynomials. In fact, it has been shown that the apparent factor of two advantage of the Gaussian quadrature rules over the Clenshaw-Curtis quadrature rule has not been found in practice [13].

For the slab coordinates case, the error in the Chebyshev Polynomial Expansion is shown in Table 2.7 below. The lowest error relative to the Ganapol results was $1.4143*10^{-6}$, and corresponds to the configuration of 7501 mesh points and either 90 or 100 Chebyshev points. The lowest error relative to the Olson results was $1.2868*10^{-6}$, and corresponds to a configuration of 7501 mesh points and 60 Chebyshev points.

Table 2. 7 Chebyshev Polynomial Expansion Error for Infinite Slab Case

Configuration	Error Relative Ganapol	Error Relative Olson	Configuration	Error Relative Ganapol	Error Relative Olson
50 Chebyshev Points 2501 Mesh Points	3.2803E-06	4.6006E-06	80 Chebyshev Points 5001 Mesh Points	1.6556E-06	1.6012E-06
60 Chebyshev Points 2501 Mesh Points	1.5457E-06	1.8820E-06	90 Chebyshev Points 5001 Mesh Points	1.5094E-06	1.3561E-06
70 Chebyshev Points 2501 Mesh Points	2.9250E-06	3.2020E-06	100 Chebyshev Points 5001 Mesh Points	1.5276E-06	1.4624E-06
80 Chebyshev Points 2501 Mesh Points	1.6103E-06	1.5180E-06	50 Chebyshev Points 7501 Mesh Points	1.4908E-06	1.3686E-06
90 Chebyshev Points 2501 Mesh Points	5.4400E-06	6.2834E-06	60 Chebyshev Points 7501 Mesh Points	1.4207E-06	**1.2868E-06**
100 Chebyshev Points 2501 Mesh Points	4.4992E-06	4.5814E-06	70 Chebyshev Points 7501 Mesh Points	1.4338E-06	1.3323E-06
50 Chebyshev Points 5001 Mesh Points	1.4969E-06	1.4000E-06	80 Chebyshev Points 7501 Mesh Points	1.4783E-06	1.3449E-06
60 Chebyshev Points 5001 Mesh Points	1.7586E-06	1.9226E-06	90 Chebyshev Points 7501 Mesh Points	**1.4143E-06**	1.3097E-06
70 Chebyshev Points 5001 Mesh Points	1.5516E-06	1.6353E-06	100 Chebyshev Points 7501 Mesh Points	**1.4143E-06**	1.2940E-06

The error for the infinite spherical coordinates case is shown in Table 2.8 below. For the spherical case, the Chebyshev Polynomial Expansion method was used for the third and fifth integrals in equation (2.53), while the Clenshaw-Curtis quadrature rule was used for the first integral. Here, the lowest error relative to the Ganapol results was $1.9532*10^{-8}$ for a configuration of 90 Chebyshev points and 2501 mesh points. The lowest error relative to the Olson results was $6.1645*10^{-8}$, for the same configuration of 90 Chebyshev points and 2501 mesh points. The fairly large difference in the errors is again due to the typo in the Olson solution at the point six mean free times and four mean free paths.

Table 2. 8 Chebyshev Polynomial Expansion Error for Infinite Spherical Coordinates Case

Configuration	Error Relative Ganapol	Error Relative Olson	Configuration	Error Relative Ganapol	Error Relative Olson
50 Chebyshev Points 2501 Mesh Points	4.4701E-08	7.3541E-08	80 Chebyshev Points 5001 Mesh Points	2.4381E-08	6.3049E-08
60 Chebyshev Points 2501 Mesh Points	3.5066E-08	6.6909E-08	90 Chebyshev Points 5001 Mesh Points	2.4152E-08	6.2748E-08
70 Chebyshev Points 2501 Mesh Points	2.2608E-08	6.3504E-08	100 Chebyshev Points 5001 Mesh Points	2.3921E-08	6.2338E-08
80 Chebyshev Points 2501 Mesh Points	1.9814E-08	6.2412E-08	50 Chebyshev Points 7501 Mesh Points	2.5568E-08	6.3510E-08
90 Chebyshev Points 2501 Mesh Points	**1.9532E-08**	**6.1645E-08**	60 Chebyshev Points 7501 Mesh Points	2.4114E-08	6.2697E-08
100 Chebyshev Points 2501 Mesh Points	1.9814E-08	6.1666E-08	70 Chebyshev Points 7501 Mesh Points	2.4191E-08	6.2833E-08
50 Chebyshev Points 5001 Mesh Points	2.4944E-08	6.3145E-08	80 Chebyshev Points 7501 Mesh Points	2.4191E-08	6.2842E-08
60 Chebyshev Points 5001 Mesh Points	2.5892E-08	6.3735E-08	90 Chebyshev Points 7501 Mesh Points	2.4114E-08	6.2715E-08
70 Chebyshev Points 5001 Mesh Points	2.5276E-08	6.3413E-08	100 Chebyshev Points 7501 Mesh Points	2.3921E-08	6.2644E-08

2.3.3 *Comparison of Numerical Integration Methods*

Comparing the relative errors for the numerical integration routines for the infinite slab case, we find that the Chebyshev Polynomial Expansion method gives the lowest relative error. However, the Chebyshev method needed significantly more mesh points to obtain the lower error. When similar configurations are compared, it becomes apparent that the Chebyshev polynomial expansion method gives a lower error than the Gauss-Legendre quadrature rule in most cases.

Comparing the relative errors for the numerical integration routines for the infinite spherical coordinates case, we find that the Chebyshev Polynomial Expansion method once again gives the lowest relative error. However the Gauss-Legendre quadrature rule gives a lower error for small numbers of quadrature points. For instance, at 2501 mesh points and 50 quadrature or Chebyshev points, the Gauss-Legendre quadrature rule gives an error relative to Ganapol's results of $3.2803*10^{-8}$, while the Chebyshev expansion method gives an error relative to Ganapol's results of $4.4701*10^{-8}$.

References

1. Duderstadt and G.A. Moses. Inertial Confinement Fusion. New York: John Wiley & Sons, 1982.

2. Atzeni, Stefano and Jurgen Meyer-ter-vehn. The Physics of Inertial Fusion. Oxford: Oxford University Press, 2004.

3. Lindl, John D. Inertial Confinement Fusion: The Quest for Ignition and Energy Gain Using Indirect Drive. New York: Springer-Verlag, 1998.

4. Henderson, D. L. and C. W. Maynard. "Time-Dependent Single-Collision Kernels for Integral Transport Theory." *Nuclear Science and Engineering*, v 102, pg 172-182 (1989).

5. Kholin, S. A. "Certain Exact Solutions of the Nonstationary Kinetic Equation Without Taking Retardation Into Account." *USSR Computational Mathematics and Mathematical Physics*, v 4, pg 213-221 (1964).

6. Wolfram, S., 1999. Mathematica 4.0: A System for doing Mathematics by Computer. Addison-Wesley, New York.

7. Lewin, Leonard. Polylogarithms and Associated Functions. New York: Elsevier North Holland Inc., 1981

8. Davis, Philip J. and Philip Rabinowitz. Methods of Numerical Integration. New York: Academic Press, 1975.

9. Ganapol, B. D., P. W. McKenty, and K. L. Peddicord. "The Generation of Time-Dependent Neutron Transport Solutions in Infinite Media." *Nuclear Science and Engineering*, v 64, pg. 317-331 (1977).

10. Olson, K. R. and D. L. Henderson. "Numerical Benchmark Solutions for Time-Dependent Neutral Particle Transport in One-dimensional Homogeneous Media Using Integral Transport." *Annals of Nuclear Energy*, v 31, pg 1495-1537 (2004).

11. Ganapol, B. D. "Reconstruction of the Time-Dependent Monoenergetic Neutron Flux from Moments." *Journal of Computational Physics*, v 59, pg. 468-483 (1985).

12. Anita, H. M. Numerical Methods for Scientists and Engineers. Boston: Birkhauser Verlag, 2002.

13. Trefethen, Lloyd N. "Is Gauss Quadrature Better Than Clenshaw-Curtis?" *SIAM Review*, submitted for publication. Retrieved from http://web.comlab.ox.ac.uk/oucl/work/nick.trefethen/ April 25th, 2007.

14. Press, William H. et al. Numerical Recipes in Fortran. Cambridge: Cambridge University Press, 1989.

Appendix A. Subtraction of Singularity

Consider an integral with a singularity at some point x_o. The idea of subtraction of singularity is to extract the singular part of the integrand. This is done by subtracting, from the integrand, an expression integrable in closed form, which eliminates the singularity and yields a form which can be integrated numerically [8]. For instance, consider

$$I(q)=\int_0^q \frac{e^{-x}dx}{1-x} \qquad 0\le q\le 1 \tag{A.1}$$

The integrand has a singularity at $x = 1$, and $I(1)=\infty$. However, we can subtract the singularity in the following manner:

$$\begin{aligned} I(q)&=\int_0^q \frac{e^{-x}dx}{1-x}=e^{-1}\int_0^q \frac{dx}{1-x}+\int_0^q\left(\frac{e^{-x}}{1-x}-\frac{e^{-1}}{1-x}\right)dx \\ &=-e^{-1}\ln(1-q)+\int_0^q\left(\frac{e^{-x}}{1-x}-\frac{e^{-1}}{1-x}\right)dx \end{aligned} \tag{A.2}$$

The first integral is evaluated analytically. The second integral has no singularity, since it equals zero at $x = 1$, and can be evaluated numerically over the whole range.

Now consider the infinite slab geometry case. The expression for the n^{th} shape factor, in terms of the $(n\text{-}1)^{\text{th}}$ shape factor is:

$$F_n(\eta)=\frac{n}{2}\left[\int_{-1}^{\eta} K_{n,A}(\eta,\eta')F_{n-1}(\eta')d\eta'+\int_{\eta}^{1} K_{n,B}(\eta,\eta')F_{n-1}(\eta')d\eta'\right] \tag{A.3}$$

where $K_{n,A}(\eta,\eta')$ and $K_{n,B}(\eta,\eta')$ are the kernels, and are calculated as:

$$K_{n,A}(\eta,\eta') = \int_0^{\frac{1-\eta}{1-\eta'}} \frac{(\tau')^{n-1}}{(1-\tau')} d\tau' = \ln(1-\eta') - \ln(\eta-\eta') - \sum_{i=2}^{n} \frac{1}{i-1}\left(\frac{1-\eta}{1-\eta'}\right)^{i-1} \tag{A.4}$$

and

$$K_{n,B}(\eta,\eta') = \int_0^{\frac{1+\eta}{1+\eta'}} \frac{(\tau')^{n-1}}{(1-\tau')} d\tau' = \ln(1+\eta') - \ln(\eta'-\eta) - \sum_{i=2}^{n} \frac{1}{i-1}\left(\frac{1+\eta}{1+\eta'}\right)^{i-1} \tag{A.5}$$

The kernels have a singularity at the point $\eta' = \eta$. To apply the subtraction of singularity method, we need to ensure that the form of the integrand that is extracted is integrable in closed form, and that the integral calculated numerically is equal to zero at the singularity. Rewriting equation (A.3) as

$$F_n(\eta) = \frac{n}{2}\left[\begin{array}{l} F_{n-1}(\eta)\int_{-1}^{\eta} K_{n,A}(\eta,\eta')d\eta' + \int_{-1}^{\eta} K_{n,A}(\eta,\eta')\left[F_{n-1}(\eta') - F_{n-1}(\eta)\right]d\eta' + \\ \qquad F_{n-1}(\eta)\int_{\eta}^{1} K_{n,B}(\eta,\eta')d\eta' + \int_{\eta}^{1} K_{n,B}(\eta,\eta')\left[F_{n-1}(\eta') - F_{n-1}(\eta)\right]d\eta' \end{array}\right] \tag{A.6}$$

fulfills the above requirements. The first and third integrals, which contain a singularity at $\eta' = \eta$, can be performed analytically. Meanwhile, the second and fourth integrals, which cannot be performed analytically, equal zero at the point $\eta' = \eta$.

Appendix B. Numerical Integration Routines

B.1 Gauss-Legendre Quadrature

While Newton-Cotes formulas, such as the Simpson's rule, are based on evaluations of a function at equally spaced points, Gaussian quadrature rules evaluate a function at points picked so that the rule is exact for polynomials of as high a degree as possible. The general form of a Gaussian quadrature rule on an interval [-1,1] is

$$\int_{-1}^{1} W(x) f(x) dx \approx \sum_{i=1}^{n} c_i f(x_i) \tag{B.1}$$

where the choice of the points x_i, the weights c_i depend on the number of quadrature points n, and $W(x)$ is the weight function and is equal to 1 for Gauss-Legendre quadrature. The quadrature rule is exact for polynomials of degree up to $2n - 1$ [12].

When the integration is performed on an interval of $[a,b]$ instead of [-1,1], the quadrature rule must be modified. Using a change of variables, it can be shown that the quadrature points t_i on the interval $[a,b]$, corresponding to the quadrature points x_i on [-1,1] can be found from [12]:

$$t_i = \frac{1}{2}\left((b-a)x_i + b + a\right). \tag{B.2}$$

Therefore, the Gaussian quadrature rule is applied to the integral

$$\int_{-1}^{1} f\left(\frac{1}{2}\left((b+a)t + b + a\right)\right)\frac{b-a}{2} dt . \tag{B.3}$$

Since the points at which the function must be evaluated for the Gauss-Legendre quadrature rule are not necessarily the same as the points at which the function is known, an interpolation scheme must be used to evaluate the function. For the Gauss-Legendre quadrature rule, a 2nd order polynomial interpolation scheme was implemented [14].

B.2 Chebyshev Polynomial Expansion

Chebyshev polynomials are a set of orthogonal polynomials, $T_n(x)$. They are defined on the real line from –1 to 1, or in θ space from 0 to 2π. The Chebyshev polynomials can be obtained from [12]:

$$T_n(x) = \cos(n \arccos x) \tag{B.4}$$

Chebyshev polynomials can also be generated from the recurrence relation [12]:

$$T_0(x) = 1 \quad T_1(x) = x \quad T_{n+1}(x) = 2xT_n(x) - T_{n-1}(x) \tag{B.5}$$

The polynomial $T_n(x)$ will have n zeros in the range [-1,1], defined as [14]:

$$x = \cos\left(\frac{\pi\left(i - \frac{1}{2}\right)}{n}\right) \quad i = 1,2,\ldots,n \tag{B.6}$$

If the function to be approximated is defined on an arbitrary range [a,b], rather than [-1,1], then a variable change can be used to make the expansion valid on [a,b]:

$$y = \frac{x - \frac{1}{2}(b+a)}{\frac{1}{2}(b-a)}. \tag{B.7}$$

Chebyshev expansion of a function involves finding a set of coefficients, c_i, for the polynomials T_i such that [14]:

$$f(x) \approx \left[\sum_{i=1}^{N} c_i T_{i-1}(x) \right] - \frac{1}{2} c_1 \tag{B.8}$$

where N is the number of Chebyshev polynomials used in the approximation, and is on the order of 30 to 50 [14]. The coefficients, c_i, are found through the following relation [14]:

$$\begin{aligned} c_i &= \frac{2}{N} \sum_{k=1}^{N} f(x_k) T_{j-1}(x_k) \\ &= \frac{2}{N} \sum_{k=1}^{N} f\left[\cos\left(\frac{\pi\left(k - \frac{1}{2}\right)}{N} \right) \right] \cos\left(\frac{\pi(i-1)\left(k - \frac{1}{2}\right)}{N} \right) \Bigg] \end{aligned} \tag{B.9}$$

If the coefficients for the Chebyshev expansion are known, the coefficients, a_i, of the equivalent polynomial in x can be found from Clenshaw's recurrence relations [12, 14]:

$$\begin{aligned} & a_i = c_i + 2x a_{i+1} - a_{i+2} \quad i = m, m-1, \ldots, 2 \\ & a_{m+1} = a_{m+2} = 0 \\ & f(x) \equiv a_0 = \frac{1}{2} c_1 + x a_2 - a_3 \end{aligned} \tag{B.10}$$

The number of Chebyshev coefficients used for the evaluation procedure can be truncated from the number of coefficients used in the expansion.

Given the coefficients c_i of the Chebyshev expansion approximating $f(x)$, it is a simple matter to calculate the coefficients, C_i, that approximate the integral of the function $f(x)$ [14]:

$$C_i = \frac{c_{i-1} - c_{i+1}}{2(i-1)} \quad i > 1 . \tag{B.11}$$

Generally, the function to be evaluated is not known at the zeros of the Chebyshev polynomial. In this case, interpolation must be performed to find the value of the functions at the zeros of the Chebyshev polynomials. A linear interpolation scheme was implemented [14].

The Chebyshev Polynomial method of performing an indefinite integral on a function is then as follow:

1) Obtain the coefficients, c_i, of the Chebyshev polynomial expansion of the function $f(x)$ using equation (B.9).
2) Obtain the coefficients of the integrated function, C_i, from the coefficients c_i using equation (B.11).
3) Evaluate the integrated function in x using equations (B.10).

Equation (B.11) is the basis of a quadrature rule known as the Clenshaw-Curtis quadrature. This quadrature rule can be used for definite integrals, using the following formula

$$\int_a^b f(x)dx = (b-a)\left[\frac{1}{2}c_1 - \frac{1}{3}c_3 - \frac{1}{15}c_5 - \Lambda - \frac{1}{(2k+1)(2k-1)}c_{2k+1} - \Lambda\right] \tag{B.12}$$

The Chebyshev Polynomial Expansion method and Clenshaw-Curtis quadrature, since they use Chebyshev zeroes as the nodes, are only exact for polynomials of degree n, as opposed to the Gaussian quadrature rules, which are exact for polynomials of degree $2n$-1. However, this factor of two advantage in efficiency is rarely seen in practice [13].

Appendix C. Derivation of Shape Factor Equations at η = 0 for Infinite Spherical Medium

This appendix gives the detailed derivation of the shape factor equations at the point $\eta = 0$ for the infinite spherical medium with isotropic scattering problem. We begin the discussion with the equation for the n^{th} collided shape factor equation, corresponding to equation (3.53) in Chapter 3, Section 3.2.1:

$$\begin{aligned} F_n(\eta) = \frac{n}{2}\Bigg[&\int_0^{\eta} K_{n,A}(\eta,\eta')\frac{\eta'}{\eta}\left[F_{n-1}(\eta') - F_{n-1}(\eta)\right]d\eta' + F_{n-1}(\eta)\int_0^{\eta} K_{n,A}(\eta,\eta')\frac{\eta'}{\eta}d\eta' \\ &+ \int_{\eta}^{1} K_{n,B}(\eta,\eta')\frac{\eta'}{\eta}\left[F_{n-1}(\eta') - F_{n-1}(\eta)\right]d\eta' + F_{n-1}(\eta)\int_{\eta}^{1} K_{n,B}(\eta,\eta')\frac{\eta'}{\eta}d\eta' \\ &- \int_0^{1} K_{n,C}(\eta,\eta')\frac{\eta'}{\eta}\left[F_{n-1}(\eta') - F_{n-1}(\eta)\right]d\eta' - F_{n-1}(\eta)\int_0^{1} K_{n,C}(\eta,\eta')\frac{\eta'}{\eta}d\eta' \Bigg] \end{aligned} \quad \text{(C.1)}$$

where the kernels are given by

$$K_{n,A}(\eta,\eta') = \int_0^{\frac{1-\eta}{1-\eta'}} \frac{(\tau')^{n-2}}{1-\tau'}d\tau' = \ln(1-\eta') - \ln(\eta-\eta') - \sum_{i=3}^{n}\frac{1}{n-2}\left(\frac{1-\eta}{1-\eta'}\right)^{n-2} \quad \text{(C.2)}$$

$$K_{n,B}(\eta,\eta') = \int_0^{\frac{1+\eta}{1+\eta'}} \frac{(\tau')^{n-2}}{1-\tau'}d\tau' = \ln(1+\eta') - \ln(\eta'-\eta) - \sum_{i=3}^{n}\frac{1}{n-2}\left(\frac{1+\eta}{1+\eta'}\right)^{n-2} \quad \text{(C.3)}$$

$$K_{n,C}(\eta,\eta') = \int_0^{\frac{1-\eta}{1+\eta'}} \frac{(\tau')^{n-2}}{1-\tau'}d\tau' = \ln(1+\eta') - \ln(\eta'+\eta) - \sum_{i=3}^{n}\frac{1}{n-2}\left(\frac{1+\eta}{1+\eta'}\right)^{n-2} \quad \text{(C.4)}$$

and where the integrals of the kernels are given by

$$\int_0^{\eta} K_{3,A}(\eta,\eta')\eta' d\eta' = \frac{\eta}{2} - \frac{\eta^2}{2} + \frac{(1-\eta)^2}{2}\ln(1-\eta) - \frac{\eta^2}{2}\ln(\eta) \quad \text{(C.5)}$$

$$\int_{\eta}^{1} K_{3,B}(\eta,\eta')\eta' d\eta' = -\frac{1}{2} + \frac{\eta^2}{2} - \frac{(1+\eta)^2}{2}\ln(1+\eta) + \frac{(\eta^2-1)}{2}\ln(1-\eta) + (1+\eta)\ln 2 \tag{C.6}$$

$$\int_{0}^{1} K_{3,C}(\eta,\eta')\eta' d\eta' = -\frac{1}{2} + \frac{\eta}{2} - \frac{\eta^2}{2}\ln(\eta) + \frac{(\eta^2-1)}{2}\ln(1+\eta) + (1-\eta)\ln 2 \tag{C.7}$$

for n = 3 and

$$\begin{aligned}\int_{0}^{\eta} K_{n,A}(\eta,\eta')\eta' d\eta' = {} & (1-\eta^2)\ln(1-\eta) - \frac{\eta^2}{2}\ln(\eta) + \sum_{i=5}^{n}\left[-\frac{(1-\eta)}{(i-2)(i-3)} + \right. \\ & \left. \frac{(1-\eta)^2}{(i-2)(i-4)} - \frac{(1-\eta)^{i-2}}{(i-2)(i-3)(i-4)}\right]\end{aligned} \tag{C.8}$$

$$\begin{aligned}\int_{\eta}^{1} K_{n,B}(\eta,\eta')\eta' d\eta' = {} & \frac{\eta^2}{4} - \frac{1}{4} + \frac{(\eta^2-1)}{2}\ln(1-\eta) + \frac{(1-\eta^2)}{2}\ln 2 + \sum_{i=5}^{n}\left[\frac{(1+\eta)}{(i-2)(i-3)} \right. \\ & \left. - \frac{(1+\eta)^2}{(i-2)(i-4)} + \frac{(1+\eta)^{i-2}}{(i-3)(i-4)2^{i-3}}\right.\end{aligned} \tag{C.9}$$

$$\begin{aligned}\int_{0}^{1} K_{n,C}(\eta,\eta')\eta' d\eta' = {} & \frac{\eta^2}{4} - \frac{1}{4} + \frac{(\eta^2-1)}{2}\ln(1+\eta) + \frac{(1-\eta^2)}{2}\ln 2 + \\ & \sum_{i=5}^{n}\left[\frac{(1-\eta)^{i-2}}{(i-2)}\left(\frac{2^{4-i}-1}{(i-4)} - \frac{2^{3-i}}{(i-3)}\right)\right]\end{aligned} \tag{C.10}$$

for $n \geq 4$.

The above derived expressions are not enough to numerically solve the spherical case infinite medium problem, because there is a singularity at $\eta = 0$. Therefore, the limit of F_n as $\eta \to 0$ must be computed. Plugging in $\eta = 0$ for the n = 1 shape factor results in $0/0$, or indeterminate. Applying L'Hospital's gives

$$F_1(0) = \lim_{\eta\to 0}\left[\frac{1}{2\pi\eta}\ln\left(\frac{1+\eta}{1-\eta}\right)\right] = \frac{\frac{d}{d\eta}\ln\left(\frac{1+\eta}{1-\eta}\right)}{2\pi\frac{d}{d\eta}\eta} = \frac{1}{\pi} \tag{C.11}$$

Again, with the $n = 2$ shape factor plugging in $\eta = 0$ results in the indeterminate relation. Again applying L'Hospital's yields

$$\begin{aligned}
F_2(0) = \lim_{\eta\to 0}\Bigg\{\frac{1}{2\pi\eta}\Bigg[&\pi^2\eta + \frac{3}{2}(1-\eta)\ln\left(\frac{1-\eta}{2}\right)^2 - \frac{3}{2}(1+\eta)\ln\left(\frac{1+\eta}{2}\right)^2 + \\
&3(1-\eta)\mathrm{Li}_2\left(\frac{1-\eta}{2}\right) - 3(1+\eta)\mathrm{Li}_2\left(\frac{1+\eta}{2}\right)\Bigg]\Bigg\} = \\
&\frac{1}{2\pi\frac{d}{d\eta}\eta}\frac{d}{d\eta}\Bigg[\pi^2\eta + \frac{3}{2}(1-\eta)\ln\left(\frac{1-\eta}{2}\right)^2 - \frac{3}{2}(1+\eta)\ln\left(\frac{1+\eta}{2}\right)^2 + \\
&3(1-\eta)\mathrm{Li}_2\left(\frac{1-\eta}{2}\right) - 3(1+\eta)\mathrm{Li}_2\left(\frac{1+\eta}{2}\right)\Bigg] = \frac{\pi}{4}
\end{aligned} \tag{C.12}$$

Next, the equation for the shape factors for $n \geq 3$ at $\eta = 0$ will be determined. The derivation begins by taking the limit of equation (C.1):

$$\begin{aligned}
\lim_{\eta\to 0}\Big\{F_n(\eta) = \\
&\frac{n}{2}\Bigg[\int_0^{\eta} K_{n,A}(\eta,\eta')\frac{\eta'}{\eta}\left[F_{n-1}(\eta') - F_{n-1}(\eta)\right]d\eta' + F_{n-1}(\eta)\int_0^{\eta} K_{n,A}(\eta,\eta')\frac{\eta'}{\eta}d\eta' \\
&+ \int_{\eta}^{1} K_{n,B}(\eta,\eta')\frac{\eta'}{\eta}\left[F_{n-1}(\eta') - F_{n-1}(\eta)\right]d\eta' + F_{n-1}(\eta)\int_{\eta}^{1} K_{n,B}(\eta,\eta')\frac{\eta'}{\eta}d\eta' \\
&- \int_0^{1} K_{n,C}(\eta,\eta')\frac{\eta'}{\eta}\left[F_{n-1}(\eta') - F_{n-1}(\eta)\right]d\eta' - F_{n-1}(\eta)\int_0^{1} K_{n,C}(\eta,\eta')\frac{\eta'}{\eta}d\eta'\Bigg]\Big\}
\end{aligned} \tag{C.13}$$

From equation (C.13), it is immediately apparent that the first and second integrals are equal to zero in the limit as $\eta \to 0$. Therefore, equation (C.13) simplifies, in the limit that $\eta \to 0$, to

$$F_n(0)=$$
$$\frac{n}{2}\left[\int_0^1 \left[F_{n-1}(\eta')-F_{n-1}(0)\right]\lim_{\eta\to 0}\frac{K_{n,B}(\eta,\eta')}{\eta}\eta' d\eta' + F_{n-1}(0)\lim_{\eta\to 0}\int_\eta^1 \frac{K_{n,B}(\eta,\eta')}{\eta}\eta' d\eta' \right. \qquad \text{(C.14)}$$
$$\left. -\int_0^1 \left[F_{n-1}(\eta')-F_{n-1}(0)\right]\lim_{\eta\to 0}\frac{K_{n,C}(\eta,\eta')}{\eta}\eta' d\eta' - F_{n-1}(0)\lim_{\eta\to 0}\int_0^1 \frac{K_{n,C}(\eta,\eta')}{\eta}\eta' d\eta'\right]$$

For the specific case where $n = 3$, the kernels at $\eta = 0$ are

$$K_{3,B}(0,\eta') = \ln(1+\eta') - \ln(\eta') - \frac{1}{1+\eta'} \qquad \text{(C.15)}$$

$$K_{3,C}(0,\eta') = \ln(1+\eta') - \ln(\eta') - \frac{1}{1+\eta'} \qquad \text{(C.16)}$$

The kernels are equal at $\eta = 0$. Therefore, subtracting the third integral from the first integral in equation (C.14) results in the indeterminate relation. Once again, L'Hospital's rule can be used and gives

$$\int_0^1 \left[F_2(\eta')-F_2(0)\right]\eta' \lim_{\eta\to 0}\frac{\left[K_{3,B}(\eta,\eta')-K_{3,C}(\eta,\eta')\right]}{\eta} d\eta' =$$
$$\int_0^1 \left[F_2(\eta')-F_2(0)\right]\eta' \lim_{\eta\to 0}\frac{\frac{d}{d\eta}\left[K_{3,B}(\eta,\eta')-K_{3,C}(\eta,\eta')\right]}{\frac{d}{d\eta}\eta} d\eta' = \qquad \text{(C.17)}$$
$$\int_0^1 \left[F_2(\eta')-F_2(0)\right]\eta' \frac{2}{(1+\eta')\eta'} d\eta'$$

The integrated kernels in the limit that $\eta \to 0$, for $n = 3$ are

$$\lim_{\eta\to 0}\int_\eta^1 K_{3,B}(\eta,\eta')\eta' d\eta' = -\frac{1}{2} + \ln 2 \qquad \text{(C.18)}$$

$$\lim_{\eta\to 0}\int_0^1 K_{3,C}(\eta,\eta')\eta' d\eta' = -\frac{1}{2} + \ln 2 \qquad \text{(C.19)}$$

Again, the integrals of the kernels are equal. Therefore, subtracting the fourth integral from the second integral in equation (C.14) results in an indeterminate. Once again, L'Hospital's rule is used:

$$F_2(0)\lim_{\eta\to 0}\frac{1}{\eta}\left[\int_{\eta}^{1} K_{3,B}(\eta,\eta')\eta'\,d\eta' - \int_{0}^{1} K_{3,C}(\eta,\eta')\eta'\,d\eta'\right] =$$

$$F_2(0)\lim_{\eta\to 0}\frac{\dfrac{d}{d\eta}\left[\int_{\eta}^{1} K_{3,B}(\eta,\eta')\eta'\,d\eta' - \int_{0}^{1} K_{3,C}(\eta,\eta')\eta'\,d\eta'\right]}{\dfrac{d}{d\eta}\eta} = 2F_2(0)\ln 2 \tag{C.20}$$

Therefore, the equation for the $n = 3$ shape factor at $\eta = 0$ is:

$$F_3(0) = \frac{3}{2}\left[2F_2(0)\ln 2 + \int_{0}^{1}[F_2(\eta') - F_2(0)]\eta'\frac{2}{(1+\eta')\eta'}\,d\eta'\right] \tag{C.21}$$

These same steps can be applied to determine the equation to be solved for $F_4(0)$. Start again by examining the kernels for $n = 4$ when $\eta = 0$.

$$K_{4,B}(0,\eta') = \ln(1+\eta') - \ln(\eta') - \frac{1}{1+\eta'} - \frac{1}{(1+\eta')^2} \tag{C.22}$$

$$K_{4,C}(0,\eta') = \ln(1+\eta') - \ln(\eta') - \frac{1}{1+\eta'} - \frac{1}{(1+\eta')^2} \tag{C.23}$$

Again, subtracting the third integral from the first integral results in the indeterminate relation. Applying L'Hospital's rule yields

$$\int_0^1 [F_3(\eta') - F_3(0)]\eta' \lim_{\eta\to 0} \frac{[K_{4,B}(\eta,\eta') - K_{4,C}(\eta,\eta')]}{\eta} d\eta' =$$

$$\int_0^1 [F_3(\eta') - F_3(0)]\eta' \lim_{\eta\to 0} \frac{\frac{d}{d\eta}[K_{4,B}(\eta,\eta') - K_{4,C}(\eta,\eta')]}{\frac{d}{d\eta}\eta} d\eta' = \tag{C.24}$$

$$\int_0^1 [F_3(\eta') - F_3(0)]\eta' \left(\frac{2}{\eta'} - \frac{2}{1+\eta'} - \frac{2}{(1+\eta')^2} \right) d\eta'$$

Taking the limits of the integrals of the kernels as $\eta \to 0$,

$$\lim_{\eta\to 0} \int_\eta^1 K_{4,B}(\eta,\eta')\eta' \, d\eta' = -\frac{1}{4} + \frac{\ln 2}{2} \tag{C.25}$$

$$\lim_{\eta\to 0} \int_0^1 K_{4,C}(\eta,\eta')\eta' \, d\eta' = -\frac{1}{4} + \frac{\ln 2}{2} \tag{C.26}$$

As in the n = 3 case, the integrals of the kernels are equal to each other at $\eta = 0$. Subtracting the fourth integral from the second integral again results in the indeterminate relation. Once again L'Hospital's rule may be applied, and results in

$$F_3(0) \lim_{\eta\to 0} \frac{1}{\eta} \left[\int_\eta^1 K_{4,B}(\eta,\eta')\eta' \, d\eta' - \int_0^1 K_{4,C}(\eta,\eta')\eta' \, d\eta' \right] =$$

$$F_3(0) \lim_{\eta\to 0} \frac{\frac{d}{d\eta}\left[\int_\eta^1 K_{4,B}(\eta,\eta')\eta' \, d\eta' - \int_0^1 K_{4,C}(\eta,\eta')\eta' \, d\eta' \right]}{\frac{d}{d\eta}\eta} = F_3(0) \tag{C.27}$$

Finally, the equation to be solved for n = 4 is

$$F_4(0) = 2\left[F_3(0) + 2\int_0^1 [F_3(\eta') - F_3(0)]\eta' \left(\frac{1}{\eta'} - \frac{1}{1+\eta'} - \frac{1}{(1+\eta')^2} \right) d\eta' \right]. \tag{C.28}$$

This same procedure can be applied to find the equation that must be solved at $\eta = 0$ for $n \geq 5$. First look at the expressions for the kernels at $\eta = 0$:

$$K_{n,B}(0,\eta') = \ln(1+\eta') - \ln(\eta') - \sum_{i=3}^{n} \frac{1}{(i-2)(1+\eta')^{i-2}} \tag{C.29}$$

$$K_{n,C}(0,\eta') = \ln(1+\eta') - \ln(\eta') - \sum_{i=3}^{n} \frac{1}{(i-2)(1+\eta')^{i-2}} \tag{C.30}$$

As in the cases with n = 3 and n = 4, the kernels are equal to each other at $\eta = 0$. Subtracting the third integral from the first in equation (C.14) results in the indeterminate relation. Once again, apply L'Hospital's rule to obtain

$$\begin{aligned}
&\int_0^1 [F_{n-1}(\eta') - F_{n-1}(0)]\eta' \lim_{\eta \to 0} \frac{[K_{n,B}(\eta,\eta') - K_{n,C}(\eta,\eta')]}{\eta} d\eta' = \\
&\qquad \int_0^1 [F_{n-1}(\eta') - F_{n-1}(0)]\eta' \lim_{\eta \to 0} \frac{\frac{d}{d\eta}[K_{n,B}(\eta,\eta') - K_{n,C}(\eta,\eta')]}{\frac{d}{d\eta}\eta} d\eta' = \\
&\qquad 2\int_0^1 [F_{n-1}(\eta') - F_{n-1}(0)]\eta' \left(\frac{1}{\eta'} - \sum_{i=3}^{v} \frac{1}{(i-2)(1+\eta')^{i-2}} \right) d\eta'
\end{aligned} \tag{C.31}$$

The final step is to examine the integrals of the kernels at $\eta = 0$.

$$\lim_{\eta \to 0} \int_\eta^1 K_{n,B}(\eta,\eta')\eta' \, d\eta' = -\frac{1}{4} + \frac{\ln 2}{2} + \sum_{i=5}^{n} \left[\frac{i-2-2^{i-3}}{(i-2)(i-3)(i-4)2^{i-3}} \right] \tag{C.32}$$

$$\lim_{\eta \to 0} \int_0^1 K_{n,C}(\eta,\eta')\eta' \, d\eta' = -\frac{1}{4} + \frac{\ln 2}{2} + \sum_{i=5}^{n} \left[\frac{i-2-2^{i-3}}{(i-2)(i-3)(i-4)2^{i-3}} \right] \tag{C.33}$$

Once again, the integrals of the kernels are equal to each other in the limit that $\eta \to 0$. Subtracting the fourth integral from the second in equation (C.14) again results in the indeterminate relation. Applying L'Hospital's rule yields

$$\begin{aligned}
&F_{n-1}(0)\lim_{\eta\to 0}\frac{1}{\eta}\left[\int_{\eta}^{1}K_{n,B}(\eta,\eta')\eta'\,d\eta' - \int_{0}^{1}K_{n,C}(\eta,\eta')\eta'\,d\eta'\right] = \\
&\qquad F_{n-1}(0)\lim_{\eta\to 0}\frac{\dfrac{d}{d\eta}\left[\displaystyle\int_{\eta}^{1}K_{n,B}(\eta,\eta')\eta'\,d\eta' - \int_{0}^{1}K_{n,C}(\eta,\eta')\eta'\,d\eta'\right]}{\dfrac{d}{d\eta}\eta} = \\
&\qquad F_{n-1}(0)\sum_{i=5}^{n}\left[\frac{(i-2)\left(16+2^{i}(i-5)\right)}{(i-3)(i-4)2^{i}}\right]
\end{aligned} \tag{C.34}$$

Finally, the equation that must be solved at $\eta = 0$ for the case of $n \geq 5$ is

$$\begin{aligned}
F_{n}(0) = \frac{n}{2}\Bigg[&F_{n-1}(0)\sum_{i=5}^{n}\left[\frac{(i-2)\left(16+2^{i}(i-5)\right)}{(i-3)(i-4)2^{i}}\right] + \\
&2\int_{0}^{1}\left[F_{n-1}(\eta') - F_{n-1}(0)\right]\eta'\left(\frac{1}{\eta'} - \sum_{i=3}^{v}\frac{1}{(i-2)(1+\eta')^{i-2}}\right)d\eta'\Bigg].
\end{aligned} \tag{C.35}$$